GLOBAL SCALE DRIVERS AND FUTURE PROJECTIONS OF THE TERRESTRIAL WATER BUDGET

by

Sarah M. Ambrose

Submitted in partial fulfilment of the requirements
for the degree of Master of Science

at

Dalhousie University
Halifax, Nova Scotia
December 2015

TABLE OF CONTENTS

LIST OF TABLES

LIST OF FIGURES

ABSTRACT

Projected changes in the hydrological cycle have raised significant concern over future water availability and the sustainability of the world's terrestrial ecosystems. In Chapter 2, I used a recently compiled dataset of observed terrestrial evapotranspiration (ET) to estimate global fields of ET as a function of land-cover (LC) type and meteorological variables. I determined the primary driving variables to be temperature, precipitation and short-wave radiation through statistical analysis and found that these relationships varied by LC type. In Chapter 3, I analyzed global climate model data to examine projected changes in the terrestrial hydrological budget; in particular, the regional balance between precipitation, runoff, and evapotranspiration. To diagnose hydrologically significant change, I applied the concept of 'climate departure' which compares the size of the projected trend to the magnitude of historical variability. I then used the climate departure analysis to test and demonstrate support for the controversial hypothesized pattern of change, known as 'wet-get-wetter, dry-get-drier' (WWDD), whereby regions with characteristically high (low) available water receive more (less) precipitation input under climate change. In particular, I develop a spatial meta-analysis framework across individual models which demonstrates stronger support for WWDD than previously recognized. The results of this thesis provide new insights into the observed drivers of hydrological flux (Chapter 2) and model-based projections of future change (Chapter 3). Such knowledge is critical for understanding the hydrological consequences of environmental change now and into the future.

LIST OF ABBREVIATIONS USED

BAR	Barren land
BIC	Bayesian Information Criterion
CRI	Irrigated Agriculture
CRN	Non-irrigated Agriculture
DBF	Deciduous Broadleaf Forest
DNF	Deciduous Needle leaf Forest
EBF	Evergreen Broadleaf Forest
ENF	Evergreen Needle leaf forest
ET	Evapotranspiration
ET_LMM	Predicted Rates of ET using the Linear Mixed Effect Model
ET_OBS	Observed ET
GCM	Global Circulation Models
GETA 2.0	Global ET Assembly 2.0
GRS	Grassland
GRZ	Grazing land
HMO	Human Modified
HWS	Human Water Security
IPCC	Intergovernmental Panel on Climate Change
LAK	Lakes and Inundated Lands
LC	Land-cover
LMM	Linear Mixed Effect Model
LOOCV	Leave One Out Cross Validation
MXF	Mixed Forest
NCC	**N**CEP/NCAR **C**orrected by **C**RU
NPP	Net Primary Production
P	Precipitation
R	Runoff
RCP4.5	Radiative forcing of 4.5 Wm^{-2}
RCP8.5	Radiative forcing of 8.5 Wm^{-2}
SAV	Savannah
SHR	Shrub land
TET	Total Evapotranspiration
TPL	Tree plantations
WTL	Wetlands

ACKNOWLEDGMENTS

I would first like to thank my supervisor, Dr. Shannon Sterling, who provided me the opportunity to complete my Masters, even while I moved out of country and started a new full time job. In addition to being so flexible, I'd like to thank her for her insight and guidance during my first foray into science. I'd also like to thank my committee, Dr. Mike Dowd and Dr. Lawrence Plug, for providing their time and insight which have improved this thesis. I'd lastly like to thank Greg, for his tireless editing, conversations, pancake making, and support; without which this thesis would never have been completed. And Mr. Sub – I can't even imagine what this thesis would be without Mr. Sub.

CHAPTER 1 INTRODUCTION

1.1 PROBLEM STATEMENT AND BACKGROUND

The Earth's upper crust and atmosphere contain approximately 1.4 x 10^6 km^3 of water that is distributed among the oceans, land, air and sub-surface (Bonan 2010). Due primarily to the heterogeneous distribution of temperature that varies around the freezing point of water within the Earth System (which allows water to exist in liquid, solid and gas phases) (Elsner et al. 2010), water evaporates from open water and soil and transpires from plant tissues (i.e., evapotranspiration) on the earth surface and is precipitated throughout the troposphere, giving rise to a vertical return flux which completes a planetary scale hydrological cycle that continuously moves water between Earth's hydrological reservoirs (Brutsaert 2008).When evaporation occurs, energy is absorbed as latent heat in the phase transition and is subsequently released to the atmosphere during precipitation (Monteith 1965). In many areas of the world (particularly wet areas), this latent heat flux via evapotranspiration can account for more than 50% of the incident radiative energy input from the sun absorbed at the surface (Teuling et al. 2010), representing a dominant energy flux in the climate and Earth System. Due to the importance of water and surface energy budgets for a broad range of environmental processes, understanding drivers and patterns of hydrological flux is of is of great societal importance.

Because water is approximately conserved on Earth over annual scales, hydrological fluxes can be described within the context of a hydrological *budget*. The primary terrestrial fluxes in the water budget are precipitation (denoted hereafter P), evapotranspiration (ET) and runoff (R). P exceeds ET over much of the land surface, with approximately 1.1 x10^5 km^3 of water falling on the global land surface as P, and 7.1 x10^4 km^3 of water returning as terrestrial ET, with the excess R to stream and rivers that supply the ocean (Bonan 2010). The terrestrial water budget can thus be defined by the following hydrological budget equation

$$\Delta S = P\text{-}ET\text{-}R, \quad (1)$$

where ΔS represents the change in water storage, P is precipitation, ET is actual evapotranspiration ('actual' is the amount of water actually removed from the surface, as

opposed to ‘potential’: the amount of water that would evaporate if there was no limit to water supply) and R is runoff (Bonan 2010).

The globally integrated, annual-scale water budget is approximately balanced (Brutsaert 2008); however, regional budgets are often strongly out of balance, which determines local water storage, and thus regional economic potential, ecosystem functioning, and the availability of ecosystem services (Palmer et al. 2008). In areas where P is much greater than ET, we find wet climates (e.g., West Coast Canada), while conversely we find dry, arid conditions where P is close to (e.g., Mojave Desert), equal, or in rare instances, less than ET. Often water budgets are also altered to meet human needs.

On ecological and evolutionary time scales, regional patterns of this water balance give rise to distinct ecological biomes (Chapin et al. 2002) with biota specifically adapted to the hydrological conditions. In turn, biota also impact the water cycle; for example, by transpiring subterraneous water (Čermák and Prax 2009) that would otherwise be unavailable to evaporation. Furthermore, any future changes in the water balance not only impact the distribution of available water for humans, but also impact ecosystem functioning and the distribution of vegetation which may have broader societal and economic consequences (Arnell 2004).

Of all the major global-scale hydrological fluxes in Equation (1), ET is the least understood due to the complexity and nonlinearities of the governing systems, and lack of reference observations (Mueller et al. 2011). Evaporation is primarily controlled by meteorological processes (e.g., the amount of energy available), while transpiration is controlled by both meteorological processes and photosynthesis rates, determined by plant physiology (Bonan 2010). Transpiration occurs through the stomata of plants which are small (~1 mm) openings on the surface of leaves which flux CO_2 into H_2O and O_2 out of the plant interior. Due to the above mentioned regions the principle drivers of ET are still highly uncertain, and predictors likely vary in importance based on regional conditions and local vegetation (Sterling et al. 2013). For example, increased solar radiation generally increases ET as there is increased available energy to evaporate water. However, under the same conditions, different plant species may respond to solar radiation in different ways (Caldwell et al. 2007); for example, one species may increase

leaf area in response to enhanced solar input, while another plant species (perhaps with shorter roots) may quickly wilt and shut down transpiratory flux. Other metrological factors such as wind speed and the vapour pressure gradient are also important as dry air exerts a greater evaporative demand, while wind is able to move saturated air away quickly, allowing for increased flux (Yin et al. 2010).

In addition to basic uncertainties in the drivers of flux (particularly ET; Mueller et al., 2011), climate change due to the accumulation of greenhouse gases in the atmosphere has the potential to fundamentally alter the global hydrological budget and regional hydrological balances. It is predicted that the water holding capacity of the lower atmosphere (troposphere) will increase approximately 7% for every 1 degree Kelvin rise in temperature (Lambert and Webb 2008). This is predicted to cause increased evaporation in wet areas and increased aridity in dry areas. It is therefore expected that changes in the terrestrial water budget will be spatially non-uniform, with an increased disparity of P between already wet and dry areas and seasons (IPCC 2013). However, the temporal timing and spatial pattern of change in regional water balances is poorly known (Greve and Seneviratne 2015) which severely limits our ability to regionally forecast future hydrological change.

1.2 Research Problem

The broad objective of this thesis is to advance our understanding of the terrestrial hydrological cycle by better understanding drivers of hydrological flux and how the hydrological balance may change in the future. In my first research chapter (Chapter 2), I use a recently assembled empirical, global-scale database of observed terrestrial ET and meteorological/ecological variables to better understand and quantify the primary drivers of ET at the regional scale and how these drivers depend on the vegetation and land-cover in those ecosystems. The general approach of this chapter is statistical where I test predictive models constructed from a suite of candidate independent variables, rank their importance, and diagnose how these relationships vary spatially across the land surface. In the second research chapter (Chapter 3), I analyze output from computer simulations of the Earth System and examine future trends in the terrestrial hydrological budget (P, R, ET) with a focus on the regional balance of these terms. In particular, I examine how

future changes compare with historical variability, as well as testing if a popular characterization of predicted trends (wet gets wet, dry gets drier) holds true under two simulated climate change scenarios.

CHAPTER 2 GLOBAL PATTERNS OF ANNUAL EVAPOTRANSPIRATION WITH LAND-COVER TYPE: KNOWLEDGE GAINED FROM A NEW OBSERSVATION BASED DATABASE

2.1 ABSTRACT

The process of evapotranspiration (ET) plays a critical role in the Earth System, driving key land-surface processes in the energy, water and carbon cycles. Land-cover (LC) exerts multiple controls on ET, yet the global distribution of ET by LC and the related physical variables are poorly understood. The lack of quantitative understanding of global ET variation with LC begets considerable uncertainties regarding how ET and key land-surface processes will change alongside ongoing anthropogenic LC transformations. Here we apply statistical analysis and models to a new global ET database (GETA 2.0) to advance our understanding of how annual actual ET varies with LC type. We derive one-degree resolution global fields for each LC using linear mixed effect models (LMM) that use geographical and meteorological variables as possible independent regression variables; the fields then are disaggregated by five-minute LC rasters. Our inventory of ET observations reveals important gaps in spatial coverage that overlie hotpots of global change. There is a bias in the spatial distribution of observations with more in mid latitudes and fewer in the high latitudes; LCs with large areas in the high latitudes such as lakes, wetlands and barren land are poorly represented. From the distribution of points, as well as the uncertainty analysis completed by bootstrapping, we identify high priority regions in need of more data collection. Our analysis of the GETA 2.0 database provides new insights into how ET varies globally, providing new empirical estimates of global ET rates for a broad range of LC types. Results reveal that different LC types give rise to distinct global patterns of ET. Furthermore, zonal ET means among LCs reveal new patterns: LCs with a higher evaporation component show higher variability of ET at the global scale, and LCs with dispersed rather than contiguous global locations have a higher variability of ET at the global scale. The zonal means also suggest that ET rates in low-latitudinal bands may be more sensitive to change than in higher latitude bands. Results from this study indicate two major advancements are required to improve our ability to predict how ET will vary with global change. First, further collection of ground

observations of ET is needed to fill gaps in LC type and spatial location identified in this paper. Second, LC types need to be de-aggregated into finer categories to better characterize ET to reduce uncertainty, as the aggregation of heterogeneous LC types into one group weakens the relation to predictor variables; this will require the development of higher-resolution LC databases.

2.2 INTRODUCTION

Evapotranspiration (ET), the land-surface flux of the water cycle, is a critical process in the Earth System that drives land-atmosphere interactions for three major global cycles, the energy, water, and carbon cycles, directly and indirectly affecting surface temperature, plant productivity, and water availability. Accurate global-scale estimates of ET are thus critical for better understanding of climatological (Shukla and Mintz 1982), hydrological (Mueller et al. 2013), and carbon interactions (Jasechko et al. 2013). However, estimations of ET made by process-based models are uncertain due to the complexity and nonlinearity of the systems governing ET as well as the lack of reference observations to validate the estimates (Mueller et al. 2011). Thus, independent global spatial fields of ET are needed for validation of Land Surface Models (LSMs), and to increase our understanding of the spatial patterns in the water cycle (Boé and Terray 2008, Seneviratne et al. 2010, Mueller et al. 2011).

Land-cover (LC) type directly influences the four major pathways that drive ET, through: a) water availability, b) energy availability, c) photosynthesis rates, and d) atmospheric moisture gradient (Sterling et al. 2013). LC change alters water availability at the land surface by changing rooting depth, changing soil properties that retain moisture, and by directly removing or adding water to the surface through inundation, draining and indirectly through irrigation. LC change alters energy availability by changing the albedo and the thermal inertia of the surface. LC change alters the atmospheric moisture gradient by altering the surface roughness and therefore surface turbulent exchange. Lastly, LC change directly alters photosynthesis rates by changing leaf area, stomatal density, water use efficiency (e.g., C3 to C4 plants) and nutrient availability.

While ET is challenging both to model and to observe, there are a range of ET datasets that have advanced our understanding of this important flux: diagnostic observation-

based datasets, reanalyses, and uncoupled or coupled land surface models (LSMs), with each having its own biases and limitations (Mueller et al. 2011, 2013). These datasets are useful in establishing global patterns of ET and determining how the patterns vary by climate type, but are not designed to estimate ET for individual LC types. To date, there is no available database designed to test the response of ET to LC change, particularly one that covers a broad range of LC types. Thus, the characterization of ET rates and patterns among different LC types has remained elusive.

Here we use a new assembly of information on point-based estimates of ET for discrete LC types to gain new insights on how ET varies with a broad range of LC types. We create and employ a database of point-based estimates of annual actual ET types (ET_OBS) and generate global fields of ET (ET_LMM) from these observations generated with a linear mixed effect model using meteorological and geographical predictors. We examine the following questions:

1 What are the patterns in available information from ET observations among LC types?
2 What are the global patterns of annual actual ET for different LC types?
3 What are the patterns of uncertainties for global predictions of ET using a statistical model among LC types?

2.3 METHODS

2.3.1 GETA 2.0 Database

The GETA 2.0 (**G**lobal **ET** **A**ssembly 2.0) database is a new global-scale dataset of annual actual ET rates classified by LC type (Table 2.1). The GETA 2.0 database comprises 2363 points across the globe representing 16 LC types (Table 2.1). GETA 2.0 has improved from its first version (in Sterling et al. 2013) through the addition of over 800 more data points. The ET values in the GETA 2.0 database (ET_OBS) include estimates covering the period 1850 to 2010, with records varying in length from 1 to 107 years. Data are collected with a variety of methods, including eddy covariance, energy balance, soil moisture balance, and water balance methods, over spatial scales ranging from plot studies to larger catchments. Criteria for inclusion in the database are that the data points were published in government or scientific literature, represent annual actual

ET, represent ET for a single LC type, and be representative of a specific location on the planet. This approach follows fundamental work begun by Helmut Lieth in the 1960s (Lieth 1972), later furthered by Olson (Olson 1975) and Atjay and coworkers (Ajtay et al. 1979), that determined characteristic net primary productivity (NPP) fluxes for the major ecosystems of the world based on a database of point observations from around the globe.

Table 2.1 LC type and annual actual ET estimation (m/yr). Type refers to LC type, whether natural (N) or anthropogenic (A). ET_LMM refers to ET statistics derived from the ET_LMM method. ET_OBS refers to ET statistics derived from the GETA 2.0 point observations.

LC type	Symbol	Type	ET_LMM (m/yr)				ET_OBS (m/yr)				Difference of Mean ET (ET_OBS-ET_LMM)
			Max	Range	Mean	Std.	Max	Range	Mean	Std.	
Evergreen broadleaf forest	EBF	N	1.56	1.22	**1.21**	0.16	3.28	3.15	**1.2**	0.39	0.01
Deciduous broadleaf forest	DBF	N	1.19	0.84	**0.75**	0.2	2.41	2.26	**0.71**	0.35	0.04
Evergreen needle leaf forest	ENF	N	1.34	1.2	**0.39**	0.16	1.5	1.41	**0.56**	0.27	-0.17
Deciduous needle leaf forest	DNF	N	0.6	0.44	**0.28**	0.05	1.95	1.84	**0.47**	0.47	-0.19
Mixed forest[1]	MXF	N	1.39	1.26	**0.34**	0.18	2.84	2.66	**0.66**	0.35	-0.32
Savannah	SAV	N	1.31	1.15	**0.78**	0.24	3.18	2.91	**0.88**	0.48	-0.1
Grassland	GRS	N	1.27	1.19	**0.42**	0.15	2.24	2.23	**0.58**	0.42	-0.16
Shrubland[2]	SHR	N	0.93	0.92	**0.31**	0.13	0.97	0.9	**0.39**	0.22	-0.08
Barren land	BAR	N	1.04	1.04	**0.07**	0.07	1.67	1.66	**0.32**	0.3	-0.25
Wetlands	WTL	N	1.94	1.82	**0.83**	0.51	4.01	3.81	**1.06**	0.64	-0.23
Lakes and Resevoirs[3]	LAK	A/N	2.59	2.46	**0.56**	0.39	3.58	3.45	**1.61**	0.74	-1.05
Irrigated cropland	CRI	A	1.5	1.11	**0.93**	0.25	4.6	4.3	**1.14**	0.79	-0.21
Non-irrigated cropland[4]	CRN	A	1.45	1.45	**0.65**	0.3	1.83	1.66	**0.62**	0.35	0.03
Tree plantations	TPL	A	1.37	1.17	**0.67**	0.37	2.5	2.37	**0.83**	0.4	-0.16
Grazing	GRZ	A	1.66	1.66	**0.66**	0.32	2.69	2.57	**0.77**	0.52	-0.11
Urban and built-up	HMO	A	1.18	1.13	**0.48**	0.17	1.13	1.02	**0.52**	0.23	-0.04

1. These are forest areas with mixed species (deciduous and evergreen).
2. Combined closed shrub land and open shrub land.
3. Includes both lakes and inundated lands, grouped together because of their shared properties.
4. The cropland dataset contains locations in desert areas which are likely erroneous. We did not remove these cells in our global ET field generation. This layer was modified to not include irrigated cropland cells.

GETA 2.0 includes both natural and anthropogenic LCs (Table 2.1). The LC classes were chosen to closely link to plant functional types commonly used in LSMs and to follow the IPCC classification scheme (Sterling and Ducharne 2008). The LC rasters have a five-minute resolution, enabling the identification of individual wetlands and urban areas, as well as major topographic and physical drivers of the local climate.

2.3.2 Model Development

2.3.2.1 Independent Predictors

Predictors that are independent of LC type were used to model global ET fields for each LC type. We used predictors from the NCC (**N**CEP/NCAR **C**orrected by **C**RU) 53-year (1948 to 2000), 6-hour, meteorological forcing dataset (Ngo-Duc et al. 2005), an elevation dataset (United States Geological Survey 1997), and latitude and longitude. The annual average values of seven meteorological predictors (Table 2.2) were extracted from the NCC dataset. The half-century timeframe of NCC captures the same timeframe in which most of the ET observational data were collected. Like other atmospheric forcing datasets, the NCC dataset is designed to describe the overlying meteorology for a variety of LC types at a particular location on the surface, and can be considered independent from LC type. It should be noted, however, that these atmospheric forcing datasets are based upon data from meteorological stations located on the surface that are typically situated on grass plots, so the atmospheric forcing data would be representative more of grass plots than any other LC type. As it is not realistic to situate meteorological stations in all the LCs for the areas that they are to represent this problem is not avoidable; although, having meteorological stations located in uniform land surface types makes it easier to interpret possible effects than would be the case if they were situated in varying LC types. There are 381 GETA 2.0 data points located on large lakes, coastal zones and islands that fall in cells not covered by rasters of the independent predictors. For points that lie on the boundary or within one degree of the NCC raster we manually moved the ET points to the nearest NCC cell from which the information was gathered for the statistical modelling of ET. For the case of large lakes, such as Lake Chad, Lake Superior and the Aral Sea that do not have dataset coverage, the elevation and NCC forcing datasets were interpolated using the nearest neighbour value at the coastline for each cell. Small oceanic islands did not have overlying meteorological data, and ET_OBS on such islands and points that were classified generally as forests were not included in the linear mixed effect modelling. Thus, of the 2363 GETA data points, 2248 were used to model the global ET_LMM fields.

Table 2.2 Independent variables tested as model predictors of ET.

Variable Name	Description	Units	Source
Precipitation	Combined rainfall and snowfall rate	kg/m	Ngo-Duc et al., 2005
Tair	Near surface air temperature at 2 m	K	Ngo-Duc et al., 2005
Qair	Near surface specific humidity at 2 m	Kg/kg	Ngo-Duc et al., 2005
Wind	Near surface wind speed at 10 m	m/s	Ngo-Duc et al., 2005
Purf	Surface Pressure	Pa	Ngo-Duc et al., 2005
Swdown	Surface incident shortwave radiation	W/m^2	Ngo-Duc et al., 2005
Lwdown	Surface incident long wave radiation	W/m^2	Ngo-Duc et al., 2005
Elevation	Land elevation	m	USGS, 2013
Lat	Latitude	Degrees	NA
Long	Longitude	Degrees	NA

2.3.2.2 Modelling Global Fields of ET

Statistical relationships were tested between ET_OBS and the independent predictors to first choose the primary independent variables and use these relationships to predict global fields of ET for each LC type. Our modeling framework was based on the linear mixed effects model (LMM) which allows for the statistical analysis of grouped data (Pinheiro and Bates 2000). The random effects take the form of LC-specific deviations to the overall slope between independent variables and ET, as described below.

We divided ET_OBS values into groups by LC type and then chose the predictors in a forward stepwise fashion using the Bayesian Information Criterion (BIC) (Kadane and Lazar 2004), where the 'best' model is the one that minimizes the BIC criterion. This criterion determined that precipitation, temperature, and shortwave radiation were the primary predictors, with precipitation and temperature having random effects (Figure 2.1). Spatial autocorrelation of the model was also tested using the Moran's I statistic and was found to be significant at the 0.05 level, therefore we updated the model to include a spherical covariance model based upon the Haversine distance for the model residuals within the 'nlme' package in R (Pinheiro and Bates 2000).

The best fit model followed (Equation 2.1):

$$\ln(ET) = Intercept_{all} + Intercept_{LC} + (TC_{all} + TC_{LC}) * Tair + (PC_{all} + PC_{LC}) * Precip + SC_{all} * SW$$

Equation 2.1

where TC_{all} is the fixed intercept for Temperature, TC_{LC} is the random effect for temperature, *Tair* is air temperature, PC_{all} is the fixed effect for precipitation, PC_{LC} is the random effect for precipitation, *Precip* is precipitation, SC_{all} is the fixed effect for *SW*, shortwave radiation; all of these parameters are normalized to z-score values. We verified there was no violation of model assumptions by checking both the homogeneity of the variance as well as the normality of the residuals within LC.

The robustness of the random effect estimates was investigated by subsetting the data and fitting individual linear models for each LC. All coefficients were of comparable magnitude and direction than the random effects estimated here.

To assess the robustness of the model predictions, we performed "leave one out cross validation" (LOOCV) (Hastie et al. 2001).We iterated the LOOCV algorithm 200 times and assessed predictive skill explicitly by LC type. The mean cross validation error showed a root mean squared error of 0.44 [lnET], but ranged nearly threefold between LCs (.339-.803 [lnET]). Histograms of the cross validation error are symmetric, indicating that the model predictions are unbiased despite high variance for some LCs.

Next, we masked the global fields of ET that were generated by the models to the 5-minute cells in which the LCs appear. (Note that the one-degree resolution of the ET_LMM predictions for each LC type does not change with this step, but shows where the LCs with this one-degree resolution ET are located within the cell). An implicit assumption here is that the major drivers of ET at the global scale that are not encompassed in the determination of the LC location are changing at a spatial rate that can be represented by a 1-degree grid (e.g., insolation, precipitation, relative humidity). While some of the finer-scale variations in topography and soils may be captured in the 5-minute LC rasters themselves, the underlying resolution of the ET_LMM rasters remains at 1-degree.

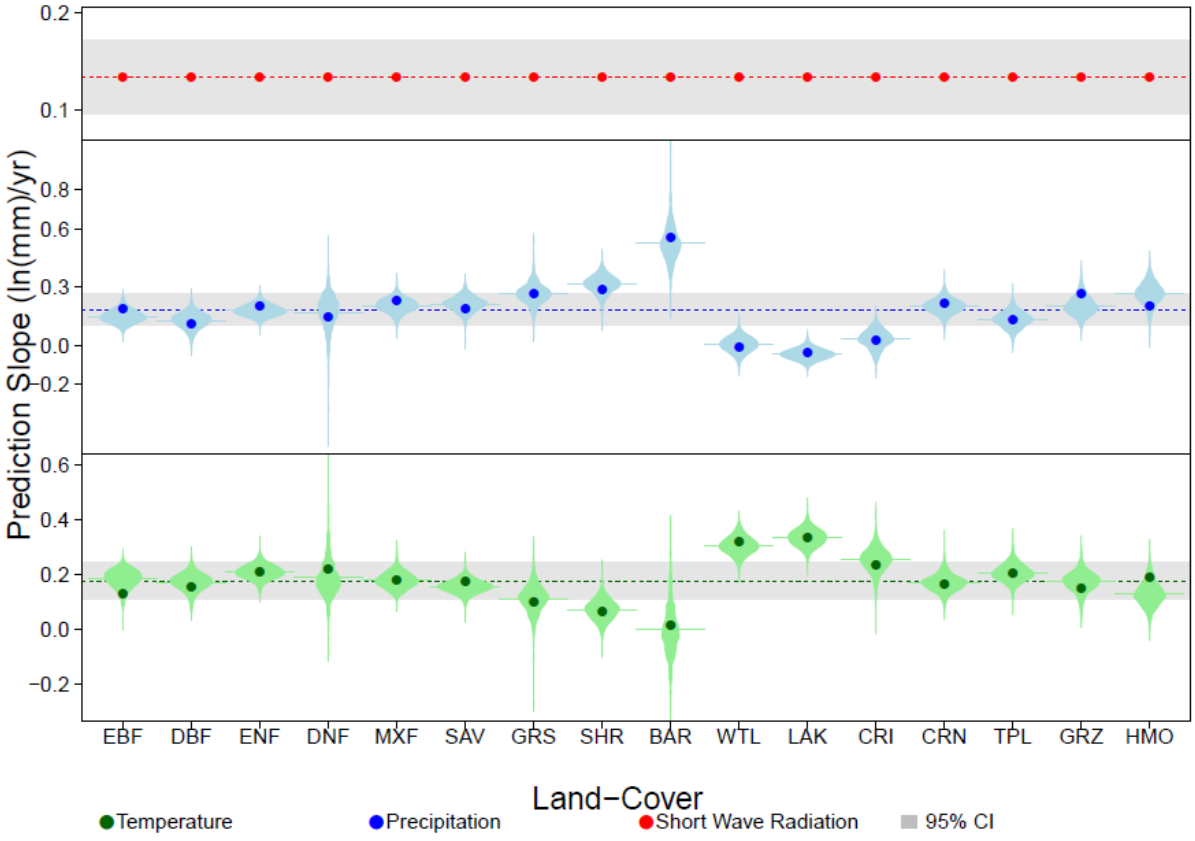

Figure 2.1 Linear mixed effect model slopes by predictor. Slopes of two random effects (i.e. slopes that vary by land- cover -precipitation (blue) and air temperature (green)) and fixed slope (common to all land-covers - shortwave radiation (red)). The fixed effect is displayed by the dotted line, with the additional random effect shown by the dot. Lighter shading indicated the bootstrapped confidence interval, where the horizontal line is the mean of the bootstrapped confidence interval.

We chose 5-minute presence/absence LC rasters used to mask ET_LMM that were derived potential and anthropogenic vegetation rasters from Ramankutty and Foley (1999) and Sterling and Ducharne (2008), except for tree plantations which was derived from Erb et al. (2007). We converted percent cover to presence/absence at the 5-minute resolution of tree plantations by preserving the area (Kröger 2012), assuming a linear tree plantation expansion rate between 1990 and 2010, with an estimate of 221.12 million hectares of tree plantations globally. The relatively fine resolution is an advantage of these LC rasters as they capture local features important in terms of climate and water budgets such as individual lakes and wetlands; however, the rasters used to mask

ET_LMM fields did not overlie neatly with the ET_OBS points, as there are cases where ET_OBS measurements were made in cells in which the LC measured was not the dominant LC; 58% of ET_OBS points did not align directly with the overlying LC raster. As we verified that the original LC classification of the ET_OBS points was correct, we included the 58% of ET_OBS that did not align with the overlying LC raster in the modelling of ET as these points represent a finer resolution LC not captured in the 5-minute rasters, rather than an error in LC classification.

To determine confidence intervals for the model coefficients and global predictions, we performed bootstrapping by randomly sampling the raw ET values within LC groups and then refit the model to generate bootstrap distributions of model coefficients and predictions (Efron and Tibshirani 1994). This was completed 1000 times to generate a distribution of possible values. We generated the distribution of estimates and the predicted ET rates 95% confidence interval by extracting the 0.025^{th} and 0.975^{th} quantiles of the bootstrapped data predictions.

2.4 Results and Discussion

2.4.1 Patterns in Available Information on Annual ET

There is a marked variation of coverage of ET observations (ET_OBS) both spatially and by LC type (Figure 2.2, 2.3); some LCs and regions in the globe have much fewer ET observations than others. Most ET observations are in forested environments (57.5 % of estimates, Figure 2.2), and of these most are in evergreen broadleaf and evergreen needle leaf forests; the exception is deciduous needle leaf forests, which have the fewest ET measurements of all LC types and also has a limited global extent, predominantly in Siberia. Barren lands and savannah have the fewest ET estimates next to deciduous needle leaf forest, followed by urban lands. As a group, anthropogenic LCs have lower

ET coverage than the natural LCs (Figure 2.2).

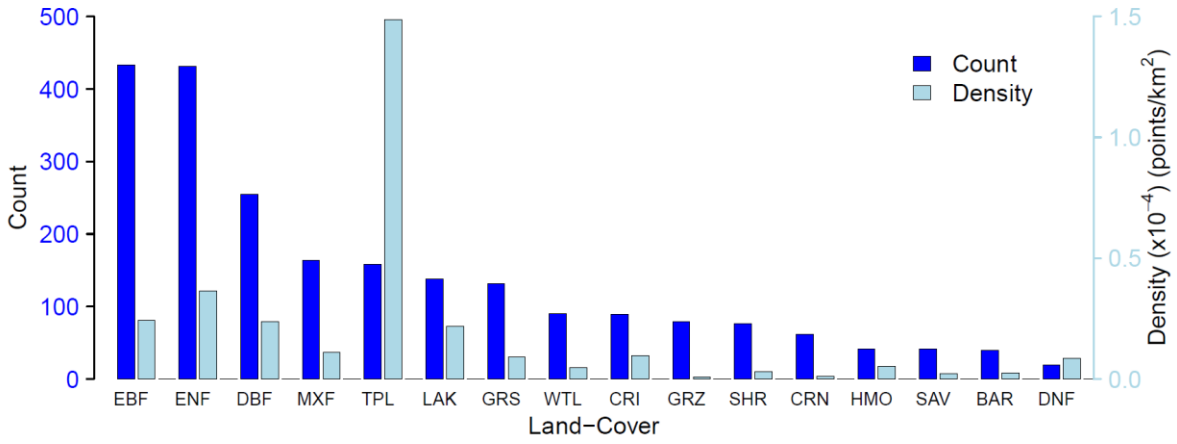

Figure 2.2 Count and density of ET measurements (ET_OBS) by LC. Count of points in the GETA 2.0 database for each LC shown in dark blue using the left axis, and the density of points for each land-cover (light blue) calculated per km^2 on the right axis (x 10^{-4}).

The spatial distribution of ET observations varies markedly across the globe (Figure 2.3). Few data points are found in Central Asia and Western Africa. Western Europe and the United States have the densest coverage of ET measurements.

Regions with lower ET_OBS coverage intersect key global hotspots. South East Asia is a hotspot for change in ET with LC change (Sterling et al. 2013, Boisier et al. 2014), for correlation of summer temperature and ET (Seneviratne et al. 2006) and for high threat to Human Water Security (HWS) (Vorosmarty et al. 2010). Equatorial Africa is a hotspot of ET change due to LC change (Sterling et al. 2013, Boisier et al. 2014), a high risk to HWS (Vorosmarty et al. 2010), and projected early temperature departure from atmospheric CO_2 increase (Mora et al. 2013). Other areas with poor ET coverage that intersect areas of high threat to HWS and change in ET from LC change include western South America, India, Eastern China and Afghanistan, Western Australia, Central America, East Africa, European Russia, Western Asia and Southern Europe.

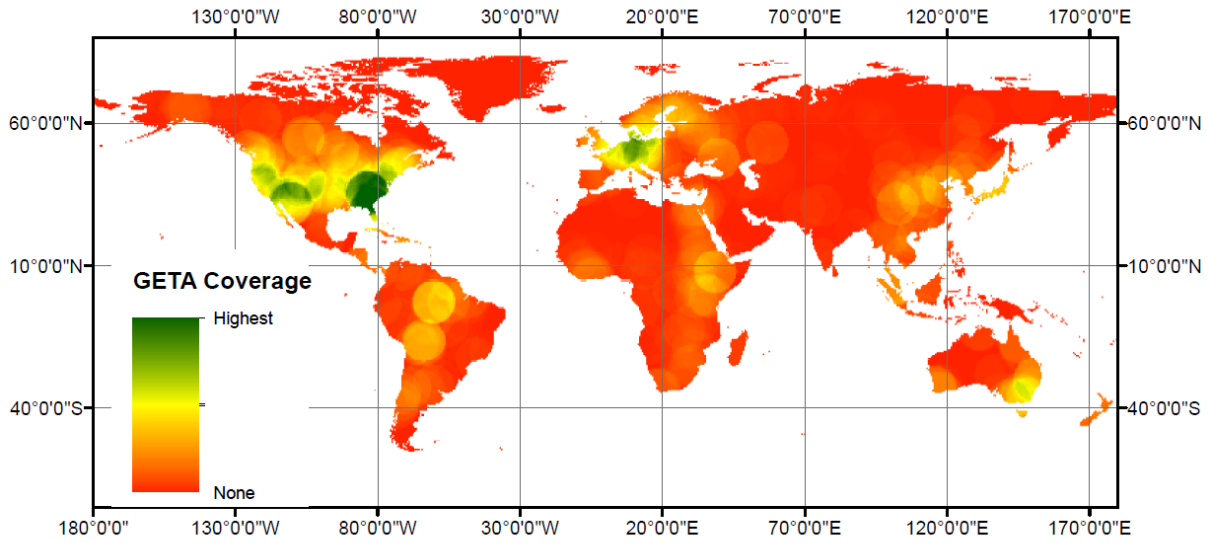

Figure 2.3 Global patterns of ET_OBS density for all LCs, as derived from the GETA 2.0 database. Circles represent the density of ET_OBS where "Highest" represents 1.26 points per 7.5 degree search radius and "None" represents zero data points per 7.5 degree search radius and "None" represents the zero data points per 7.5 degree search radius.

Our statistical model predicts that the LCs for which temperature greatly contributes to higher ET_LMM values, precipitation does not and vice versa (Figure 2.1, Table 2.3). This relationship follows the theoretical moisture versus energy-limited status of LC types (e.g., Creed et al. 2014). For example, the ET_LMM rates for barren lands (BAR, often moisture limited) increase with increasing precipitation, with almost no change with increasing temperature. Conversely, ET_LMM rates for wetlands and irrigated agriculture (by definition energy limited) increase with temperature, with almost no change with increasing precipitation. ET reacts to a more equal combination of precipitation and temperature drivers for forests, savannah, non-irrigated agriculture, tree plantations, grazing lands and urban lands.

Table 2.3 Regression coefficients estimated using a linear mixed model with spatial correlation. These estimates are for log ET across the globe; rasters used for prediction have been log transformed and standardized (z-scores) so that the slopes are directly comparable between predictors and within LCs.

	Intercept	Random Effect		Fixed Effect
		Tair	Precip	SW
All	0.64	1.19	1.2	1.14
EBF	1.2	0.95	1.00	NA
DBF	1.04	0.97	0.93	NA
ENF	1.07	1.03	1.01	NA
DNF	1.06	1.04	0.96	NA
MXF	0.99	1.00	1.04	NA
SAV	0.94	1.00	1.00	NA
GRS	0.84	0.92	1.09	NA
SHR	0.71	0.89	1.11	NA
BAR	0.55	0.85	1.44	NA
WTL	1.3	1.15	0.82	NA
LAK	1.54	1.17	0.8	NA
CRI	1.26	1.06	0.85	NA
CRN	0.98	0.99	1.03	NA
TPL	1.07	1.03	0.95	NA
GRZ	1.03	0.97	1.08	NA
HMO	0.83	1.01	1.02	NA

2.4.2 Global ET Means for Individual LCs

Our analysis reveals that the order in which terrestrial biomes have the highest to lowest ET follows the established order of biome NPP ranking (Lieth 1975, Olson et al. 1983, Saugier et al. 2001). The mean annual ET rates (for both ET_OBS and ET_LMM) are highest for evergreen broadleaf forest, irrigated croplands, and wetlands and are lowest for barren land (Figure 2.4, Table 2.1). The majority of ET_OBS lie between 0.30 and 1.5 m/yr (Figure 2.4), with the observed mean equal to 0.84 m/yr and the median equal to 0.69 m/yr.

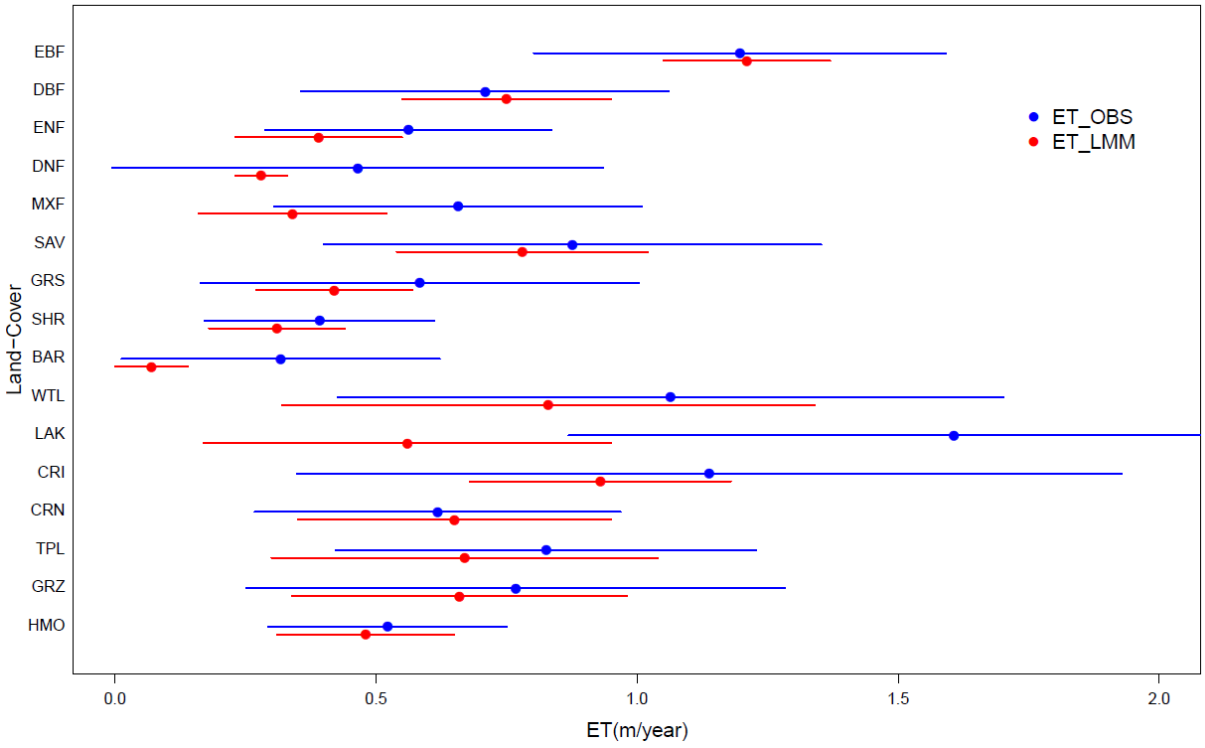

Figure 2.4 Mean (point) and standard deviation (line) for observed (blue) and standard error of annual ET values by land-cover. Observed ET values (ET_OBS) represent point observations of ET from the GETA 2.0 database and mixed effect model estimated (ET_LMM - red) represents ET of global fields generated by a statistical model from ET_OBS.

The data show that many LC types have significantly different global annual average observed ET (ET_OBS) from other LCs. Of the 120 different comparisons of ET_OBS LC types, 70 (58.3%) are significantly different at $\alpha = 0.05$ using Tukey's mean comparison test (Table 2.4). Non-irrigated agriculture and deciduous broadleaf forests are the LCs with the fewest significant differences from other LC types, these LCs have ET values in the middle range of ET (0.25 to 1.0 m/yr), with means between 0.6 to 0.7 m/yr. Lakes have a significantly higher ET rate than all other LC types.

Table 2.4 Tukey's Mean comparison test p-values for testing whether mean observed values of ET (ET_OBS) significantly varies by land-cover (LC). Significance at alpha = 0.05 level is noted by bold typeface.

	EBF	DBF	ENF	DNF	MXF	SAV	GRS	SHR	BAR	WTL	LAK	CRI	CRN	TPL	GRZ	HMO
EBF																
DBF	**0.00**															
ENF	**0.00**	**0.00**														
DNF	**0.00**	0.57	1.00													
MXF	**0.00**	1.00	0.55	0.90												
SAV	**0.00**	0.62	**0.00**	0.05	0.21											
GRS	**0.00**	0.33	1.00	1.00	0.99	**0.01**										
SHR	**0.00**	**0.00**	0.11	1.00	**0.00**	**0.00**	0.14									
BAR	**0.00**	**0.00**	0.05	1.00	**0.00**	**0.00**	0.05	1.00								
WTL	0.36	**0.00**	**0.00**	**0.00**	**0.00**	0.62	**0.00**	**0.00**	**0.00**							
LAK	**0.00**	**0.00**	**0.00**	**0.00**	**0.00**	**0.00**	**0.00**	**0.00**	**0.00**	**0.00**						
CRI	1.00	**0.00**	**0.00**	**0.00**	**0.00**	0.10	**0.00**	**0.00**	**0.00**	1.00	**0.00**					
CRN	**0.00**	0.98	1.00	0.99	1.00	0.18	1.00	0.15	**0.05**	**0.00**	**0.00**	**0.00**				
TPL	**0.00**	0.34	**0.00**	**0.05**	**0.04**	1.00	**0.00**	**0.00**	**0.00**	**0.00**	**0.00**	**0.00**	0.10			
GRZ	**0.00**	1.00	**0.01**	0.31	0.89	1.00	0.17	**0.00**	**0.00**	**0.00**	**0.00**	**0.00**	0.80	1.00		
HMO	**0.00**	0.42	1.00	1.00	0.92	**0.02**	1.00	0.98	0.74	**0.00**	**0.00**	**0.00**	1.00	**0.01**	0.19	

However, the ET comparisons based on ET_OBS data are limited by the spatial coverage of the observations. Most ET observations are located in mid-latitudes, and LCs with large areas in higher latitudes (e.g., lakes, wetlands and barren lands) are more poorly-represented by the current ET observations. As a result, the mean global average ET for these LCs derived from ET_OBS is too high. For these LCs, ET_OBS is higher than the ET_LMM mean (Table 2.1, Figure 4), as expected because ET_LMM covers the high-latitudes. The difference in maximum value for the ET_OBS and ET_LMM is greatest for lakes, barren lands and wetlands, as expected.

For other LCs, the means of ET_OBS and ET_LMM are similar, such as for evergreen broadleaf forest, deciduous broadleaf forests, savannah, shrub land, irrigated agriculture and urban lands; the location of these LCs tend to be in the mid- to low- latitudes for which there is better representation in ET_OBS. In general, the model predictions

(ET_LMM) are well within one standard deviation ET_OBS for most LCs (Table 2.1, Figure 2.4).

The GETA 2.0 ET estimates for individual LCs correspond well with another estimate (Rockström et al. 1999) that summarized mean ET for LC types, although comparisons are challenging because of lack in congruency in LC classes among studies. For the four LC types that are congruent with GETA 2.0 types, the Rockström et al. (1999) mean annual ET estimates fall within the ranges of ET_OBS and ET_LMM. We found a 9.57% median cell specific difference between results generated by a multi-tree ensemble (Jung et al. 2010) and ET_LMM, calculated at a half-degree resolution; the largest differences occurred at locations with wetlands, which was included in ET_LMM but not in Jung et al. (2010), and in these locations the ET_LMM was greater than the ET prediction in Jung et al. (2010).

Global ET_LMM fields project a cumulative total ET (TET) of 70,600 km^3/yr for a globe covered with potential vegetation), and wetlands (Figure 5). This value coheres with the range of published estimates of TET (73,000 km^3/yr (Arora 2001); 71,000 km^3/yr (Baumgartner et al. 1975); 72,900 km^3/yr (Berner 1987); 60,000 to 85,000 km^3/yr (Haddeland et al. 2011); 62,800 km^3/yr (Mu et al. 2011); 75,000 km^3/yr (Oki 1999); 56,000 to 84,000 km^3/yr (Rockström et al. 1999); and 64,500 to 72,000 km^3/yr (Mueller et al. 2013). Our analysis includes major lakes, not included in many other analyses, which may explain why our estimate lies on the higher end of the range of projected TET.

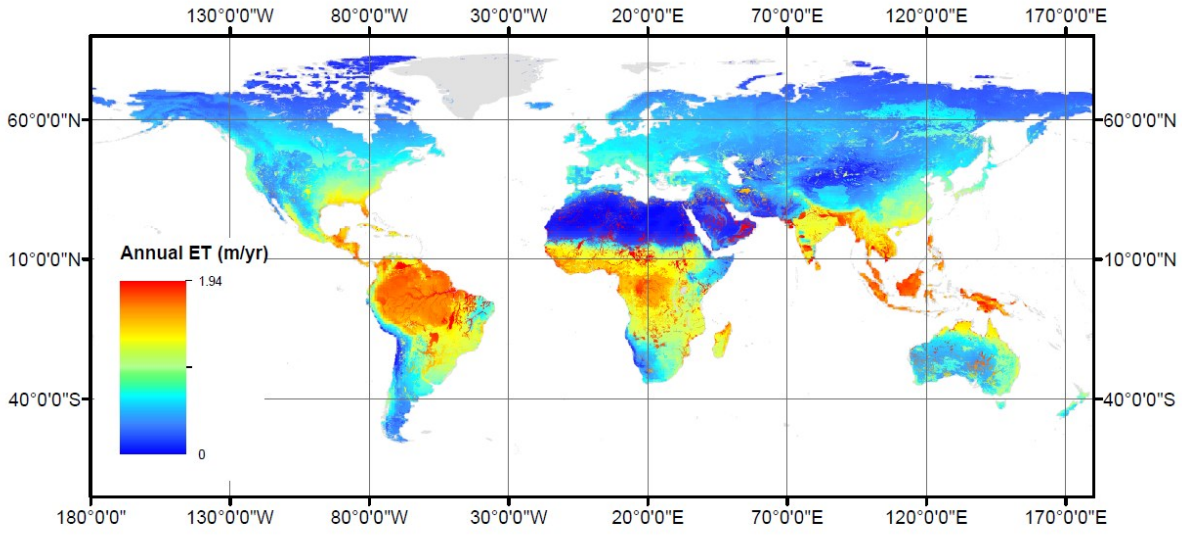

Figure 2.5 Linear Mixed Effect Model predicted rates of ET (ET_LMM) (m/yr) of global annual actual ET projections for potential vegetation (listed as Natural in Table 1) with wetland overlay. Grey indicates areas permanently covered by ice or large lakes. ET_LMM maps for individual anthropogenic land-covers are presented in Appendix A.3.

2.4.3 Zonal Patterns of ET

The modelled ET (ET_LMM) results show that different LC types have different zonal patterns of ET (Figure 2.6). LCs differ in rates as well as the shape and variability of their zonal ET means. Results indicate that lakes have the highest mean ET rates at almost all latitude bands, while deciduous needle leaf forest have the lowest (Table 2.1, Figure 2.6). Of LCs that extend across majority of the latitude bands, barren lands and shrub lands have the lowest values.

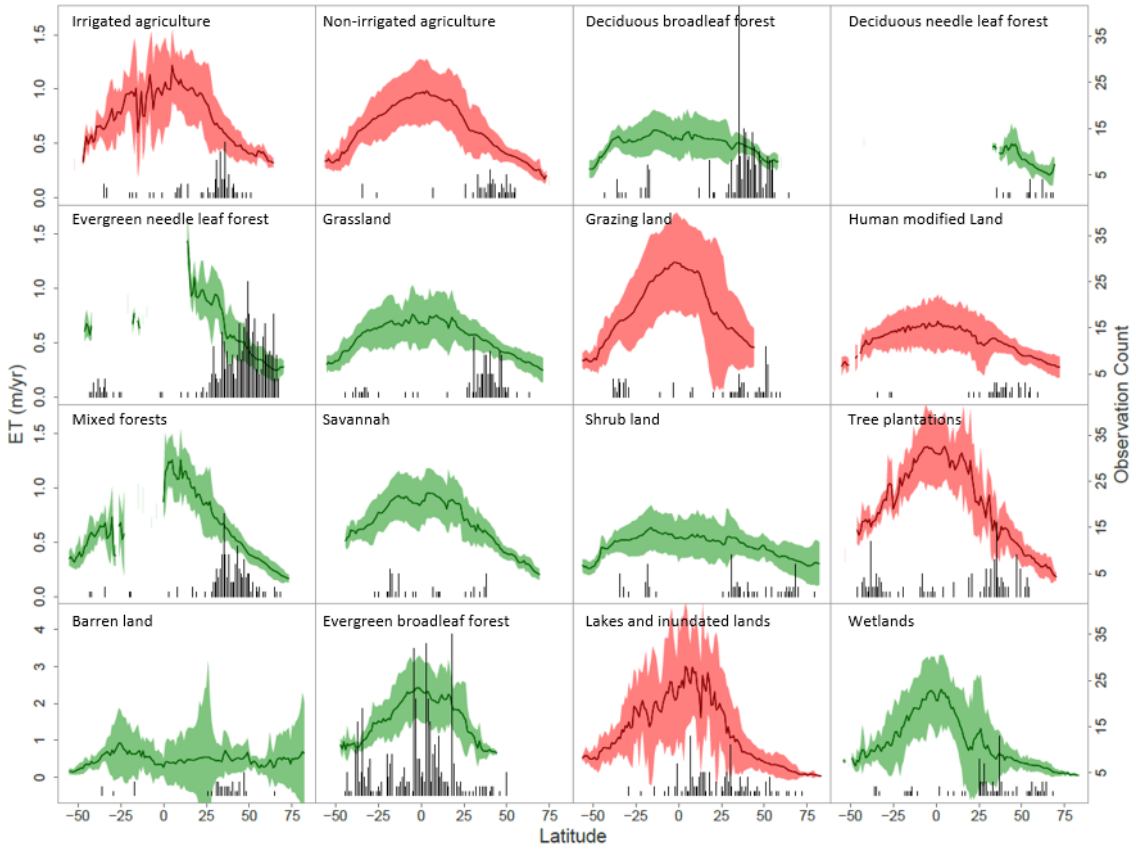

Figure 2.6 Zonal patterns of ET_LMM for LC types. The line represents the zonal mean, and the lighter area represents the 95% confidence interval derived from bootstrapping. Green represents potential vegetation (DBF, DNF, ENF, GRS, MXF, SAV, SHR, EBF, and WTL, as listed as Natural in Table 1), and red represents anthropogenic vegetation (CRI, CRN, GRZ, HMO, TPL, BAR and LAK, (here classified as anthropogenic although it is a mix of natural lakes and anthropogenic reservoirs)), See Table 1 for abbreviations). The black line plots represent the number of observations at that latitude.

The most common zonal pattern of ET shows a higher mean ET rate around the equator that declines with increasing latitude, but the shape of this relation varies with LC type. The zonal patterns reveal that LCs with highest available surface water (evergreen broadleaf forest, lakes and wetlands) also have the largest increases in ET with latitude towards the equator (Figure 2.6). In contrast, LCs with the lowest amount of available surface water (grasslands, shrub lands and barren land) have the smallest increases in ET

with latitude towards the equator. The common zonal ET shape is consistent with another study that showed for ET rates for all LCs lumped together peaking at about zero degrees latitude (Zeng et al. 2012).

The zonal plots suggest that the expected response of ET to a particular LC change is not the same across all latitudinal bands. For example, results suggest that conversion of wetlands to grazing land may decrease annual ET at the mid- and lower latitudes and the difference is most significant in the mid-latitudes (Figure 2.6). Results suggest that a change from evergreen broadleaf forest to urban lands may cause the greatest reductions in ET nearer the equator as compared with higher latitude bands. Similarly, results suggest that a change from shrub land to lakes would cause the greatest increases in ET in the low latitudes. While the zonal plots suggest likely changes to ET resulting from a variety of LC changes in particular latitude bands, given the lack of sufficient data in some latitudes and uncertainties of the ET_LMM model in these regions, further investigation is needed to verify these observations.

Results suggest that the global-scale pattern of a LC location, whether dispersed or contiguous, impacts zonal ET variability. Results show that LCs that have more contiguous global locations (e.g., non-irrigated croplands, deciduous broadleaf forests and shrub lands, Figure 2.5) have smoother zonal curves with less variability among latitude bands. In contrast, LCs with dispersed global locations (e.g., lakes, irrigated agriculture, tree plantations, and urban lands, Figure 2.5) have higher variability in mean zonal ET in adjacent latitude bands (Figure 2.6). Thus LCs with larger contiguous areal locations are expected to have more gradual changes in climate among adjacent cells, and more direct feedback over their overlying meteorology than do LCs with dispersed locations. Zonal ET_LMM confidence intervals are largest around the equator and 20-30 ^{o}N, corresponding with the latitudinal belt that includes a large range of climate types (e.g., deserts in Africa and tropical forests in SE Asia).

Results also indicate differences in global scale ET variability can also be explained by relative roles of vegetation among LC types. LC's for which ET is dominated by one of energy or moisture limitations (barren land, wetlands, and lakes, Figure 1) have more variability in their zonal patterns with wider confidence intervals around the mean

(Figure 2.6). In contrast, LCs for which ET is governed through a more equal combination of water availability and energy (such as evergreen needle leaf forest, savannah, and non-irrigated cropland, Figure 2.1) can be considered to be more vegetation-dominated; these LCs have lower variability in their zonal patterns with smaller confidence intervals around the mean (Figure 2.6). The first group of LCs are expected to have a greater role of evaporation in ET, as these LCs have more open water and bare soil; thus, a possible explanation for higher ET variability of these LCs is that they can occur in a much wider variety of climates than the vegetation-dominated LCs, and are therefore exposed to a larger range of conditions in the ET drivers. Indeed, we observe that the ranges of the independent predictors (shortwave radiation, precipitation and air temperature), normalized by the LC area, are greatest for lakes, followed by urban areas and wetlands, and that barren lands have the largest temperature and shortwave radiation range of all the LCs. For the "vegetation-dominated" LCs, the lower variability in global ET can be explained by a smaller range of climate conditions experienced per unit area of the LC, and thus these vegetation dominated LCs are exposed to a lower range of ET drivers. These relationships imply that LCs dominated by energy or moisture limitations will have more uncertainty in their projections with a statistical model from than vegetation-dominated LCs with more balanced energy and moisture limitations to ET. An exception to this observation are evergreen broadleaf forest (Figure 2.6) which is governed by a balance of both energy and moisture limitations also has a wide confidence interval; the higher than expected variability of evergreen broadleaf forest may be due to its very high ET rates or to its lower percentage of interception compared to other forest types (following Miralles et al. (2010)). Further research using more refined LC classes is needed to examine these hypotheses.

2.4.5 Uncertainties in ET for Individual LC Types

The bootstrapping results are consistent with those from cross-validation and indicate that the parameter estimates are relatively insensitive to error in the data. Again, the bootstrap distributions showed good symmetry which indicates that the fitted relationships are unbiased. Taken together, the two model diagnostics indicate relatively high variance

(largely due to sparse sampling), yet also indicate unbiased parameter estimates and predictions which indicate a robust underlying physical signal.

Confidence intervals generated using the bootstrapped models indicate that the largest uncertainties in the ET_LMM predictions lie in Africa and northern latitudes (Figure 2.7). These uncertainties qualitatively agree with the density of points generated from ET_OBS in that the lowest uncertainties are located in areas with the most points, such as North America and Europe (Figure 2.7), and the largest uncertainties lie in predictions of Africa, Southern Asia, South America and far northern locations. In terms of LC type, the largest uncertainties are associated with barren lands and wetlands (Figure 2.7).

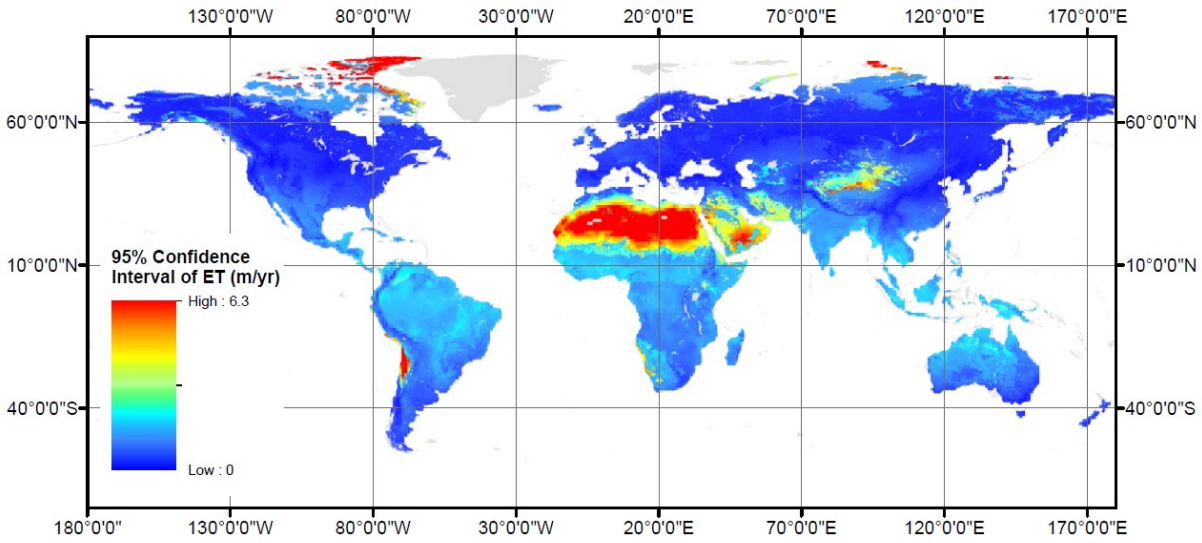

Figure 2.7 Confidence interval size for estimated rates of ET from the mixed effect model (ET_LMM) generated from 1000 bootstrapped datasets.

Reliability of ET_LMM predictions also varies with LC type due to varying levels of extrapolation in the model resulting from predictors being used outside of the ET_OBS range. We have mapped the regions of coverage for each LC type to identify the locations for which the ET predictions are less certain (Appendix A.3); some of the LCs have poorer coverage of the independent predictors by ET_OBS, leading to less accurate predictions in ET_LMM. In particular, barren land is not well covered by the predictor ranges, resulting in less certain ET predictions outside of the predictor ranges in Northern

Africa, Tibet, the Arctic and the Altiplano. These maps also serve to identify where further data collection is needed so that ET fluxes of the LCs can be better understood.

At some locations the estimates of ET_LMM result in greater rates than the input precipitation (this is not found for energy limitations). Predictions for these areas yield greater annual rates of ET than precipitation (see Appendix A.1 for a map of regions where ET > precipitation), although we chose not to adjust ET_LMM values as they are still assumed to be the best estimate from this particular model. However, we recognize that this is a limitation of the statistical model, which is not inherently constrained by physical limitations (water and energy). On the other hand, it may actually be possible for ET to exceed P for certain LCs (i.e., wetlands, lakes and inundated lands, and irrigated agriculture), due to water inputs from other regions (either anthropogenic or natural). Opposed to artificially augmenting the current model by imposing a maximum ET rate (which would violate the assumption of normally distributed model errors), we suggest explicit incorporation of physical limitations as a way to potentially improve the statistical parameterization in future work.

As mentioned earlier, the LC type of 58% of the ET_OBS points did not align with the dominant LC type in the LC raster. This discrepancy will not add error to the ET_LMM estimates, because the true LC type is considered to be the LC linked with the ET_OBS and is the one used in the LMM; however, this discrepancy does affect the ET_LMM results in that the masked ET_LMM cells will not extend over all the cells in which the LC occurs, to address this, the unmasked ET_LMM raster may be masked to a different LC raster. ET in ocean archipelagos is not well represented in the analysis, due to gaps in coverage of the independent predictors. Advances in atmospheric forcing datasets to cover ocean archipelagos are needed to address this limitation.

Taken together, our results show several pathways through which the uncertainty in global modelled annual average values of ET (ET_LMM) relates with LC type. LCs with the highest uncertainty in ET_LMM projection are those that have dispersed locations (Figure 2.5), lower point and density of coverage (Figure 2.2, 2.3), larger areas with climate conditions outside the ET_OBS range (Appendix A.3), and have a greater role of evaporation in ET. In contrast, LCs with the lowest uncertainty have more contiguous

locations, higher point and density of coverage, smaller areas with climate conditions outside the ET_OBS range, and are vegetation-dominated. For example, lakes and barren lands have a relatively high uncertainty in ET predictions and this may be explained by three things: 1) lakes and barren lands have greater decoupling of LC location from climate variables (i.e., these two LCs can occur in a greater range of climates than can tropical evergreen forest, for example), 2) lakes in particular have a spatial pattern that is comprised of disparate sub-units (i.e., more patchy) which would increase the range of conditions in the climate drivers that affect the LC, and 3) lakes and barren lands have more extensive extrapolation of ET_LMM beyond the range of predictor variables compared with other LC's, due to absence of measurements in key climate locations (such as the arctic barren lands), as shown in Appendix A.3. Future work is also recommended to extend this analysis to cover sub-annual variation, finer spatial scales, climate sub-types of LC classes, and the impact of successional stages on ET.

It should be noted that the one-degree ET rasters may be masked by other LC maps apart from the ones used for this study. Other studies that may want to compare, for example, global land surface model output of ET may use the map used in their global land surface model to mask the ET_LMM; but it should be kept in mind that the original ET data are at a one-degree resolution.

2.5 CONCLUSIONS

Our assembly and statistical analysis of the novel GETA 2.0 database provide a new characterization of global ET patterns for a broad range of LCs, building upon existing knowledge in other databases that do not classify ET by LC type. Our results show that LCs have distinctly different means and zonal patterns. Lakes have the highest ET rates across all latitude bands, although the high latitudes are particularly uncertain.

The one-degree global fields of ET produced here (ET_LMM) are useful as a reference for process-based model estimates of ET because they are derived from statistical modelling of observations, and therefore do not rely on the same assumptions used in deterministic land surface and climate models. Furthermore, information presented here on ranges of ET observations for individual LC types (Table 2.1, Figure 2.3) can be used

to support decisions on whether modeled ET outliers can be excluded based on physical considerations (e.g., McCabe et al. 2008).

Results suggest that ET may be more sensitive to LC change in some latitude bands than others. Changes to ET from LC change appear to be largest in the tropical latitude bands, particularly associated with differences between ET in LCs with high and low water availability. This finding suggests that land use planning should be particularly careful in the tropics because of the possibility of heightened impacts to the Earth System in these latitude bands; further study of these observations is recommended.

Our analysis suggests two fundamental LC characteristics affect global ET variability: contiguous LCs display smaller ET variability than dispersed LCs; and LCs that have a heightened role of evaporation in ET have higher variability in global ET than vegetation-dominated LCs. More work to further explore these hypotheses is needed to advance our ability to predict changes to ET with global change.

Our inventory of annual actual ET observations reveals regions and LC types where estimates are most lacking, and many of these are within key global change hotspots in the Arctic, Africa and central Asia. Further some LCs have much sparser ET observations than others. Anthropogenic LCs, including grazing land, non-irrigated croplands, and urban areas, are among the most poorly represented LCs by ET observations. We recommend that anthropogenic LCs be targeted for future monitoring of ET. Many anthropogenic LCs also face higher heterogeneity of overlying meteorological conditions within their LC type, related to a greater role of evaporation in ET (e.g., reservoirs), increased spatial dispersion (e.g., urban areas), or a combination of these factors (e.g., irrigated cropland). Thus it is particularly challenging to reliably project ET in anthropogenic LCs at the global scale. An added challenge is that anthropogenic LCs are also difficult to parameterize in process-based models because of their within-class heterogeneity. Division of LCs into subclasses for future modelling will help to reduce the heterogeneity needed to better define characteristic the land surface fluxes in these LCs.

Resolution is an important characteristic in any global projection of ET. For example, local high and low values of ET cancel out with coarser spatial resolutions leading to

underestimation of ET gradients within continents (Mueller et al. 2011). Because the ET_LMM generated here represents only a single climate within a grid cell, and because the ET_LMM was generated by 1-degree results disaggregated to 5 minutes by LC rasters, the range and variability in LC types and ET rates will always be lower in the model than in the real world, where diverse microclimates can harbour a greater variety of ET rates and LC types. A finer resolution scheme that accounts for more heterogeneity will allow for improved representation of the diversity of microclimates but will inevitably fall short of representing all possible microclimates and LCs.

Issues related to LC change will grow in complexity, as our land surface accumulates a more complicated history of varying types of LC change all while adjusting to changes in overlying meteorology. As LC change continues, anthropogenic LCs will play an increasingly significant role in overall global ET rates; because of the particular uncertainties in estimating ET for anthropogenic LCs, advances in modelling and observation networks of ET in human dominated areas are urgently needed. Continued advances in understanding how ET varies spatially and with LC type are necessary to improve predictions and mitigation actions for the future. The findings here on characteristic ET rates and global patterns with LC type improve our quantitative understanding of the spatial patterns in the water cycle and how ET will change with ongoing anthropogenic transformations; this fundamental information is needed for us to better understand how the earth's energy balance, carbon cycle, and water cycle will respond to global change.

CHAPTER 3 FUTURE PROJECTIONS OF DEPARTURE AND TERRESTRIAL WETTING AND DRYING IN THE CONTEXT OF HISTORICAL VARIABILITY

3.1 ABSTRACT

The hydrological cycle plays a critical role in the Earth System by driving key land-surface processes in the energy and carbon cycles, and determines the amount of available water for human and ecological use. Here we analyse Global Earth System Model output from the Coupled Model Intercomparison Project Phase 5 (CMIP5) for the terrestrial hydrological variables of precipitation, evapotranspiration (ET), and runoff to increase our understanding of how the terrestrial hydrological cycle may change under climate change. We estimate annual average rates for these variables at 0.5 degree cells between the years 2006 - 2100, and determine where predicted rates exceed the bounds of historical variability (1860-2005) using the concept of climate departure. We then determine if the historically wettest and driest locations (determined by historically averaged quantiles of the respective variables) are predicted to become wetter or drier in the future. Our analysis focuses on both the multi-model mean and inter-model variability. Results indicate strong disparities in departure dates among models, although we find that ET consistently departs first among the variables analysed. We also find that individual models strongly support the WWDD pattern (> 65% of the time). Of the 58 simulations used in calculating the predicted rates of change in flux (29 models x 2 future scenarios), 54 exhibit the WWDD pattern. Support for WWDD was also found across a continuum of historical wet/dry classifications, indicating that an extended WWDD framework may better describe future projections, where the wettest (driest) areas get wettest (driest), while intermediate wet (dry) regions show intermediate future trends, and so on. Finally, we determine that further work into inter-model variability is needed to provide robust estimates of future trends of the hydrological cycle.

3.2 INTRODUCTION

The terrestrial hydrological cycle plays a critical role in the Earth System by shaping the structure and functioning of terrestrial ecosystems, governing available water, and by regulating land surface energy budgets. Land inputs of water due to precipitation (P) are

partitioned into evapotranspiration (ET), runoff (R) and infiltration to soil moisture and groundwater. The relative magnitude and spatial pattern of these fluxes thus determines local water budgets and ultimately the quantity and distribution of available water for human use (Bonan 2010). Continued increases in radiative forcing due to greenhouse gas emissions is expected to alter regional hydrological budgets over the land surface, with increasingly severe alteration to regional budgets predicted over the 21st century due to ongoing greenhouse gas emissions (IPCC 2013). For example, Global Climate Models (GCMs) presented by the recent Intergovernmental Panel on Climate Change's Fifth Assessment (AR5) predict increasing precipitation in high northern locations and strong increases in subsequent runoff (between 1950-2010), while simultaneously predicting strong decreases in precipitation over southern Europe, the Middle East and southern Africa. These predictions indicate large regional variability that arises due to regionally-specific climate dynamics, vegetation, and land-use, among other factors (IPCC 2013 Chapter 2.5), which interact to govern regional hydrological budgets. Furthermore, variability among model predictions makes understanding the robustness of these predictions very challenging. Thus diagnosing the dominant patterns of change in these fluxes and how they may vary regionally is still a major challenge for global hydrology in order to develop a consistent picture of future change.

In terms of globally integrated quantities, total global P is generally expected to increase due to larger atmospheric water content, primarily as a function of increased temperature (Lambert and Webb 2008, Lu and Cai 2009). These projected P increases will cause greater available water for land ET and thus 'accelerate' the global hydrological cycle. However, effects of climate change on the third major flux, ET, are debated. This is due to large uncertainties with respect to the ways plant physiology and species composition will change under evolving environmental conditions. For example, transpiration may be deceased through water use efficiency (Kimball and Idso 1983), or transpiration may be enhanced due to increased leaf area due to fertilization from CO_2 (Piao et al. 2007, Gerten 2013).

Spatially variable magnitudes and interactions among these hydrological processes make understanding predicated trends in global-scale hydrological budgets challenging.

Previous research has looked at the predicted trends of individual hydrologic variables globally (for example, P (Zhang et al. 2007), R (Alkama et al. 2013), and ET (Douville et al. 2013)), while few have examined combined projections in terms of the balance of the hydrological budget and how this balance may vary regionally. An exception is the recent study by Dirmeyer et al. (2014) who recently analyzed 10 Coupled Model Intercomparison Project Phase 5 (CMIP5) models, focusing on trends in hydrological extreme events of R, P and soil moisture. They found an expected increase in droughts, with little increase in floods under the RCP4.5 climate change scenario, while they found an increase in both floods and droughts under the RCP8.5 scenario.

One innovative method for understanding climate change in the context of historical variability was introduced by Mora et al. (2013). They examined GCM output from the CMIP5 using the concept of 'climate departure', defined as the date by which a climate variable exceeds the bounds of historical variability (following Mora et al. 2013 see Methods below). Their analysis methods were based on the idea that many regions of the world have bounded climate oscillations; therefore, any climatologically significant (opposed to statistically significant) trend must exceed the limits defined by natural oscillations specific to a particular region. This concept has provided a simple yet powerful way to understand future climate change in the context of characteristic historical variability within a particular region. This distinction of the term 'significant' is important because statistically significant (opposed to climatologically significant) trends can be difficult to interpret in the context of natural climate oscillations (see Wunsch 1999 for a discussion of statistical significance of climate trends in the context of natural oscillations). This quantification is also important at a societal level as regionally-specific infrastructure is more likely adapted to historical variability, making it more important to understand changes in this historical context, rather than the absolute magnitude of trends. The analysis of Mora et al. (2013) focused on a broad suite of climate variables (including P over the ocean, global evaporation, and terrestrial transpiration); however, their results were primarily reported in terms of globally integrated trends with respect to the combined marine and terrestrial response. They also constrained departure dates to the year 2100 when none occurred, and this method was criticized in the literature

(Hawkins et al. 2014). Here we perform a more in-depth, spatially explicit departure analysis that focuses on regional and inter-model variability.

A major hypothesized pattern of future hydrological change is known as 'wet get wetter, dry get drier' (WWDD) (Chou et al. 2009, 2013, Allan et al. 2010, Greve et al. 2014, Greve and Seneviratne 2015). This pattern suggests an intensified hydrological cycle, predicted on account of enhanced convective precipitation due to high surface temperatures, leading to increased precipitation in wet and convectively active areas of the world and less future precipitation in drier subsidence regions (Held and Soden 2006, Chou et al. 2009). Several studies have provided support for seasonal patterns of WWDD over the land and ocean, with model based studies (Chou et al. 2009) and observational studies (Liu and Allan 2013). Importantly, most previous work has focused on combined land and ocean results. For example, Held and Soden (2006) point out that their work supporting WWDD in the tropics was dominated by a strong WWDD signal over the ocean. Recent work (Greve and Seneviratne 2015), has used CMIP5 model predictions to refute the WWDD mechanism based on a statistical significance framework. Their study used potential ET and aridity to quantify wet and dry areas, as opposed to actual ET due to a suggested difficulty in interpreting P-ET (actual) over land because the quantity is positive almost everywhere (and thus defined as 'wet' within their scheme). While it is true that P-ET > 0 over land cannot be used to determine the "wet" land areas, P-ET can still be used as a valuable metric to determine historically wet and dry areas if grouped by quantiles, similar to Allan et al. (2010). Furthermore, Greve and Seneviratne 2015 analyzed the multi-model mean of 30 CMIP5 models, and did not establish whether WWDD was supported within individual models. Individual model analysis may be crucial because individual models may locate wet and dry areas in different regions of the world, meaning that the multi-model average wet and dry regions may simply be an artifact of spatial averaging and have little hydrological significance.

Here we further test the WWDD pattern in CMIP5 output in the specific context of climate departure. We first seek to establish spatially explicit climate-departure statistics for each flux in the terrestrial hydrological budget (P, R and ET) and characterize model-model variability. We then apply this framework with respect to wet and dry areas of the

world (determined by P-ET) and contrast the resulting WWDD patterns with previous work based on statistical significance. We also utilize a simpler alternative definition of wet and dry areas based on historical quantiles of P-ET (actual). We use simulations over the 'historical' period (1850-2005) to characterize contemporary wet and dry areas, and two future climate change scenario simulations (representing two levels of future climate forcing between 2006-2100) of ET, R, and P to answer the following questions in the context of modern GCMs:

What are the projected future trends for terrestrial ET, R, and P at the regional and global scales?

Do predicted rates of ET, R, and P *exceed* the historical (1860-2005) bounds of variability? Do CMIP5 models predict a common departure in the terrestrial water cycle variables before 2100? Does hydrological climate departure depend on the degree of climate forcing? Are there regions or scenarios that have the most similarity between models?

Do CMIP5 models predict patterns of WWDD when analyzed using hydrological departure (note here that we use the term 'wet' to represent the large relative magnitude for each variable, while we recognize this may not correspond to area intuitively thought of as 'wet') and slope analysis calculated on historic quantiles of wet and dry regions?

Does the departure analysis suggest different patterns of WWDD than previous analyses? Do patterns of WWDD depend on the degree of climate forcing? Does support of WWDD depend on the magnitude of quantiles of wet vs. dry? Do the extreme wet and dry areas, defined as the most extreme quantiles (e.g., 5% wettest (driest)) behave differently than the moderately wet and dry areas (e.g., 40% wettest (driest))?

Do individual models simulate variable patterns of wet and dry?

Classifying this as an uncertainty analysis, how does model-model variability compare to the multi-model mean? And does this influence our conclusions regarding WWDD?

3.3 METHODS

3.3.1 Data

We analyzed historical (1860-2005) and future projections (2006-2100) within the CMIP5 ensemble for the following global-scale, spatially explicit, simulated hydrological field variables: actual evapotranspiration (ET), runoff (R) and total precipitation (P). We did not include ground water, as its role has previously proven to be negligible in year-to-year changes when compared to P, R, and ET in CMIP5 simulations (Greve and Seneviratne 2015). We included CMIP5 models which simulate the selected variables for our analysis (models listed in Appendix B.1). For future predictions we examined two of three climate scenarios specified by Representative Concentration Pathways (RCPs) (Meinshausen et al. 2011; Taylor et al. 2011). These RCPs simulate the Earth System response to different prescribed levels of future CO_2 emissions that represent an effective radiative forcing of i) high future emissions (or 'business-as-usual') giving a CO_2 equivalent radiative forcing of 8.5 Wm^{-2} (RCP8.5); ii) a midrange mitigation scenario where CO_2 emissions are reduced to give a projected radiative forcing of 4.5 Wm^{-2} (RCP4.5); and iii) an aggressive emission mitigation scenario (RCP2.5) which is now generally considered unfeasible (van Vliet et al. 2009) and was therefore not included in the analysis. The three variables of interest were downloaded from the Earth System Grid Federation. The model grid resolution varied (0.75 – 3.75 degrees) so we interpolated the data onto a common 0.5 degree grid using bilinear interpolation.

3.3.2 Hydrological Climate Departure

The departure analysis is based on the methods first introduced by Mora et al. (2013). For each region, they computed the maximum and minimum value for a variable during a historic time series, and then determined whether future simulations exceed the historic bounds when subjected to future emission scenarios (Figure 3.1). They identified the first occurrence in time for each variable within each scenario that exceeded the historical bounds as well as the time of permanent departure (until 2100). Here we applied the same method, where 'permanent departure' is defined as the first year that all subsequent years are outside of the bound of historic variability (1860-2005) until 2100. However, a main difference from our analysis and the analysis in Mora et al. (2013) is the determination of

the multi-model date of departure. Mora et al. (2013) used the average across models, assuming a departure of 2100 when none occurred; this approach has been criticized for calculating a `pseudo departure`, where variables that do not depart from the historic bounds are given a year of 2100 and for using statistical inference methods that assume climate simulations are statistically independent (Hawkins et al. 2014). Instead, we calculated the departure year at the 25th percentile across models (further described as '25% model agreement'), while no year was applied to locations and models that did not depart. To capture uncertainty in departure, we report the year where 25 and 50 % of models agree.

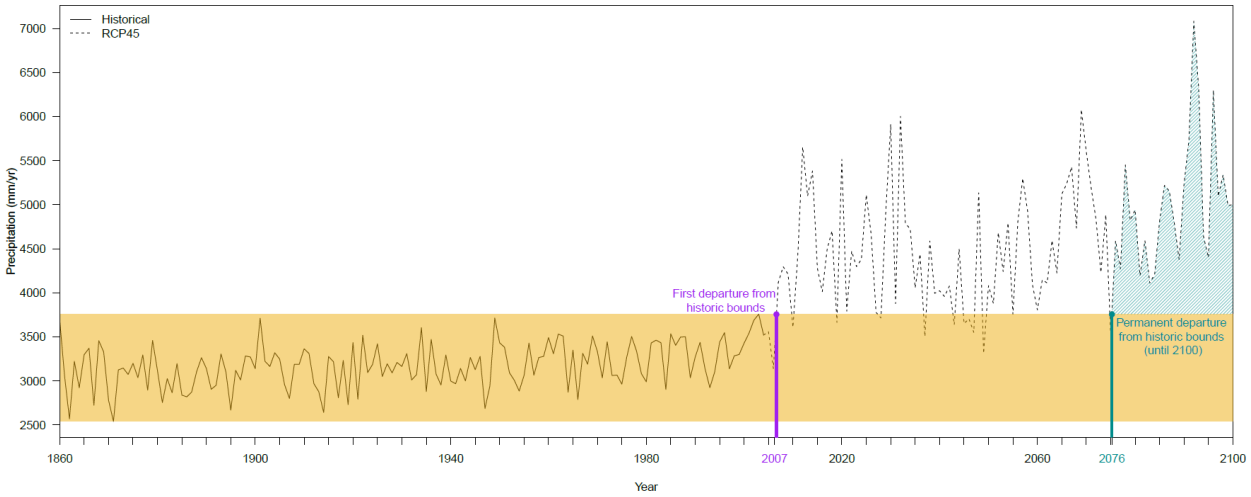

Figure 3.1 An example of estimating the first and final departure from the mean. Annual precipitations for an example grid cell of a single model (0.5 degree x 0.5 degrees) exceeds the historical bounds (yellow) for the first time (2007, purple), and permanently until 2100 (2076, teal).

3.3.3 Wet-get-wetter, dry-get-drier (WWDD)

To test and compare WWDD patterns, we first characterized the global land surface into wet and dry areas on the basis of the simulated quantiles of each respective variable (P, R, and ET) within the historical simulations. To avoid using a single quantitative threshold (as in Allan et al. 2010) we computed a range of thresholds and designate individual cells as dry (wet) depending on whether they fall within the lowest (highest) global 5, 10, 15, 20, 25, 30, and 40% quantiles of P - ET (a measure of local water availability - Greve and Seneviratne 2015) based on historical variability. By using a

range of quantile values we extend previous analyses by testing WWDD along a continuum of wetness and dryness. This allows us to test whether the historically extreme and moderate regions of P-ET behave differently in future climate regimes. This 'continuum' WWDD framework also serves as a sensitivity analysis in terms of how WWDD conclusions depend on the specific wet/dry threshold used.

We then quantify and compare WWDD patterns in two ways: i) departure, and ii) linear trends (using P-ET). For departure, we computed the percentage of the total wet (dry) area determined by the historic quantiles that depart in a wet (dry) direction, or not at all for all models (2006-2100). Secondly, the linear trend analysis determined whether wet and dry regions have a positive or negative slope with respect to time (2006-2100) in future simulations. For each quantile bin of P-ET we computed the spatially averaged future slope and determined whether its magnitude is dependent on the wetness/dryness quantile used, thus testing the continuum of WWDD. Note that unlike the departure analysis, which classifies regions into wetter, drier, or no departure, the slope analysis of P-ET categorizes regions as only becoming wetter or drier, and does not have a "no change" classification akin to the 'no departure' in the departure analysis.

3.3.4 Uncertainty Analysis

The uncertainty analysis focuses on model-model variability. We adopt a simple 'location-independent' metric to test WWDD by which we calculate as the proportion of area that confirms/denies WWDD *within models*, and then take the standard deviation of the proportion *across models*, thus defining a WWDD statistic that is independent of the actual wet/dry locations within individual models.

3.4 Results

3.4.1 Hydrological Climate Departure Analysis

In the mean global departure analysis P, R, and ET have a positive trend (Figure 3.2), showing predicted intensification of the terrestrial hydrological cycle and is consistent with an increased trend reported in the IPCC AR5 for P, ET, and R (Alkama et al. 2013). All variables under both forcing scenarios exceed the historic bounds by the year 2068, with ET for RCP4.5 (2013), RCP8.5 (2009) departing first, followed by P for RCP4.5 (2027), RCP8.5 (2034), then R for RCP4.5 (2068) and RCP8.5 (2036). For each variable,

we see that the RCP8.5 scenario exhibits a steeper predicted trend than RCP4.5 (P was 1.8 x more quickly, R was 3.3 x, and ET 1.2 x – Table 3.1), and that all variables and scenarios exceeded historic bounds in terms of the global average before 2100 (as marked on Figure 3.2). We see that the trend appears to be fairly linear between 2006-2100 for all variables and RCP scenarios, and that the RCP4.5 trends are weaker than RCP8.5.

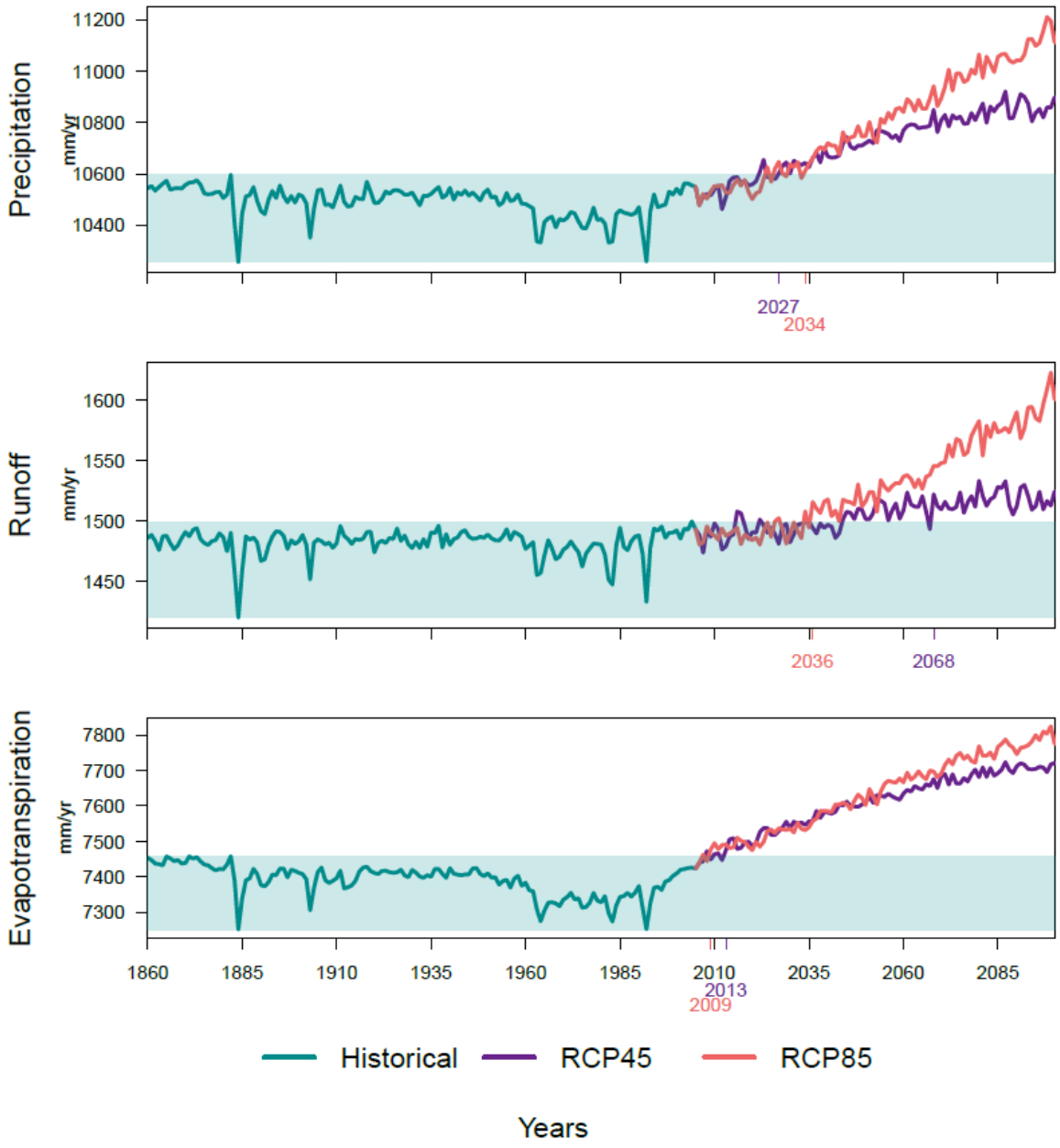

Figure 3.2 Historical (green) and projected, RCP4.5 (purple) and RCP8.5 (red) multi-model global land averages between 1860-2100 for Precipitation, Runoff, and Evapotranspiration. Years indicate the year of first year of permanent departure until 2100.

Table 3.1 Slopes of predicted mean global trends ((mm/year) year^{-1}) for all variables under RCP4.5 and RCP8.5 scenarios.

	RCP4.5	RCP8.5
Precipitation	4.06	7.24
Runoff	0.40	1.31
Evapotranspiration	2.92	3.88

The terrestrial hydrological departure analysis shows that all variables (P, R, ET and P-ET) have some locations of permanent departure until 2100 (Figure 3.3) under 25% model agreement, with all variables under the RCP4.5 and RCP8.5 scenarios departing in more than 19% of the global land area (Table 3.2). The earliest year of departure in the water cycle occurs for ET in the year 2022 under the RCP8.5 simulation. For all variables, more locations depart under the RCP8.5 scenario than RCP4.5. ET showed the smallest difference between scenarios (1.3x), and precipitation showed the largest (2.3x).

Similar to the global average (Figure 3.2), we find that ET has the largest percent of global land area that departs from historic bounds (69.83% and 92.39% for RCP4.5 and RCP8.5, respectively), while, conversely, precipitation (33.89% and 77.30%) has the least (Table 3.2) under 25% model agreement. This pattern of departure by land area where ET > P > R does not hold for the 50th percentile, where we find ET > R > P (Table 3.2). At 25% model agreement, the most prominent spatial trend in the departure analysis is a consistent lack of departure across models across the Sahara desert, and Australia. This feature is consistent for all variables but largely disappears in the RCP8.5 scenario. At 50% model agreement, there are clear patterns of departure in northern latitudes for runoff and precipitation, while ET has no similar pattern (Appendix B.2). For all variables, there is higher model agreement of departure under the RCP8.5 scenario, with each individual variable (P, R, ET) having at departure in more than 75% of the global land area under 25% model agreement, and the ET has the highest proportion of models that depart in the most locations (Figure 3.4).

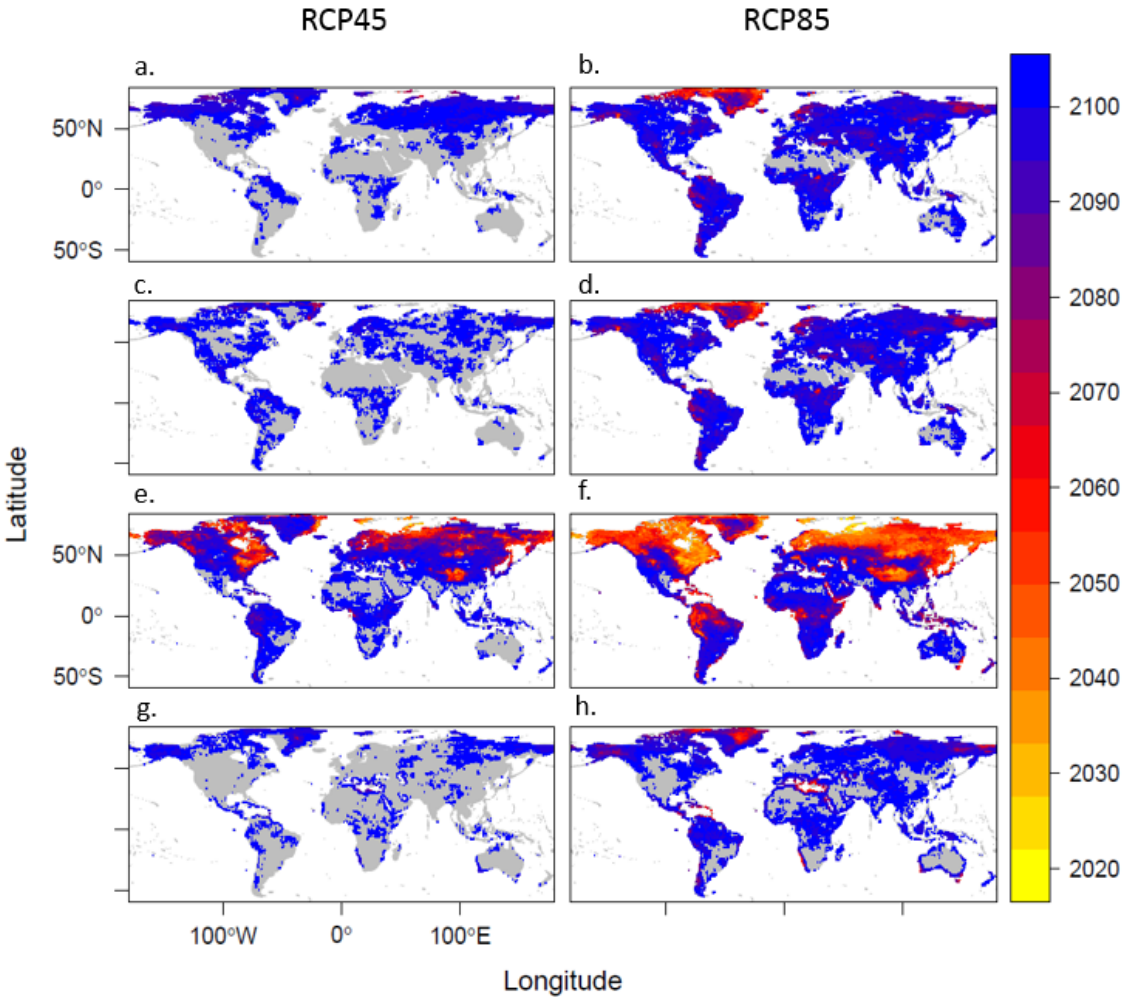

Figure 3.3 Date of historic departure when 25% of models agree for a) precipitation RCP4.5, b) precipitation RCP8.5, c) runoff RCP4.5, d) runoff RCP8.5, e) evapotranspiration RCP4.5, f) evapotranspiration RCP8.5, g) precipitation-evapotranspiration RCP4.5, and h) precipitation-evapotranspiration RCP8.5.

Table 3.2 Percentage of land area that departs up to 2100, as determined by the 25th percentile, and 50th percentile of model agreement estimates. Bolded are the largest percentages for each scenario and quantile.

	25th percentile		50th percentile	
	RCP4.5	RCP8.5	RCP4.5	RCP8.5
Precipitation	33.9	77.3	4.1	24.3
Runoff	35.1	78.8	0.2	11.4
Evapotranspiration	**69.8**	**92.4**	**26.2**	**50.6**
Precipitation-ET	19.4	57.8	0.8	13.5

The conclusions of this departure analysis (at 25% model agreement) vs. Mora et al.'s (2013) show some qualitative similarities, although results look very different at 50% model agreement (where Mora et al. (2013) show unanimous departure, and our analyses show very little). For ET, results are similar to the prediction in Mora et al. (2013) for evaporation on land where earliest departure is found at higher latitudes and the lowest departure in Africa; results differ when examining the 50% model agreement, where Mora et al. (2013) showed departure at all locations in the globe with many locations departing before 2080 under RCP8.5, we only found departure at (26.15%, 50.63% for RCP4.5 and RCP8.5, respectively) at some locations. The years of departure look similar between predicted ET results and Mora et al.'s (2013) departure of transpiration at northern locations, although again departure of transpiration was found at all of the locations (in Mora et al.'s (2013) analysis), while our analysis showed much fewer locations un under the 25% and 50% model agreement scenarios calculated here. These differences are due to the different definitions of departure. In Mora et al. (2013) they included variables that did not depart, giving them a value of 2100, while we computed the mean year at a given percentage of model agreement. Despite that many models simulate departure, there are a large percentage of models that simulate little to no departure. For example, our approach projects that no hydrological variable will depart for 100% of the global land area, whereas Mora et al. (2013) predict all locations will permanently depart. Hawkins et al. (2014) argue that limiting the upper bound to 2100 sets an artificial departure date, which is shown by how fewer locations depart using our 25% agreement method with allowable NA values.

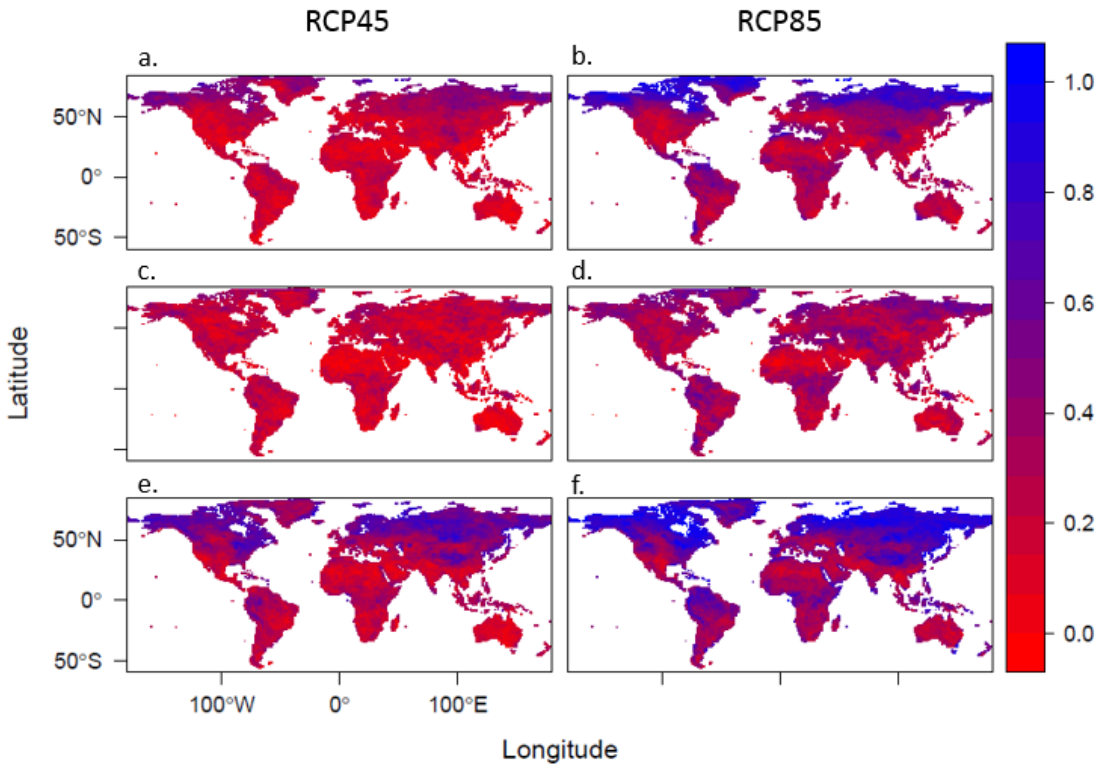

Figure 3.4 Proportion of models for each variable that have a date of permanent climate departure for a) precipitation RCP4.5, b) precipitation RCP8.5, c) runoff RCP4.5 and d) runoff RCP8.5, e) evapotranspiration RCP4.5, f) evapotranspiration RCP8.5.

3.4.2 Wet-get-wetter, dry-get-drier Analysis

The mean historical quantiles for the hydrological variables (P, R, ET) show similar spatial trends with respect to one another (Figure 3.5), with the driest (where dry represents the smallest magnitude of flux) region through the equator in Africa, central North America, and Australia. The wettest regions are located throughout Asia, South America, Central Africa and the coasts.

Both the departure and slope analysis show support for the WWDD hypothesis (Figure 3.6). The WWDD departure analysis supports the WWDD hypothesis (Figure 3.6a-d), with more than 40% of the wet quantiles exhibiting WW patterns for all variables, and more than 25% exhibiting DD patterns for P, R and ET. These rates are similar to those reported in (Greve and Seneviratne 2015), where both find support for WW in ~60 % of locations (Greve and Seneviratne 2015), although they went on to test the significance of these trends and subsequently rejected WWDD. For reasons discussed below, statistical

significance testing may be difficult to interpret in the context of diverse climate oscillations in particular regions. Furthermore, the resulting p-values from the analysis may also be difficult to interpret since there is no true statistical sampling (which p-values are based upon) when analyzing the output of a deterministic simulation. This point does not seem to have been picked up in the CMIP5 literature, but seems important and may warrant follow-up analysis and discussion. When interpreting trends in the context of the region-specific maxima and minima, results seems to more strongly support WWDD and do not depend on the interpretation of statistical p-values.

We find that there is some support for WWDD under the WWDD slope analysis (Figure 3.6f) with more than 50% of the areas exhibiting patterns of WW and DD under both the RCP4.5 and 8.5 scenarios.

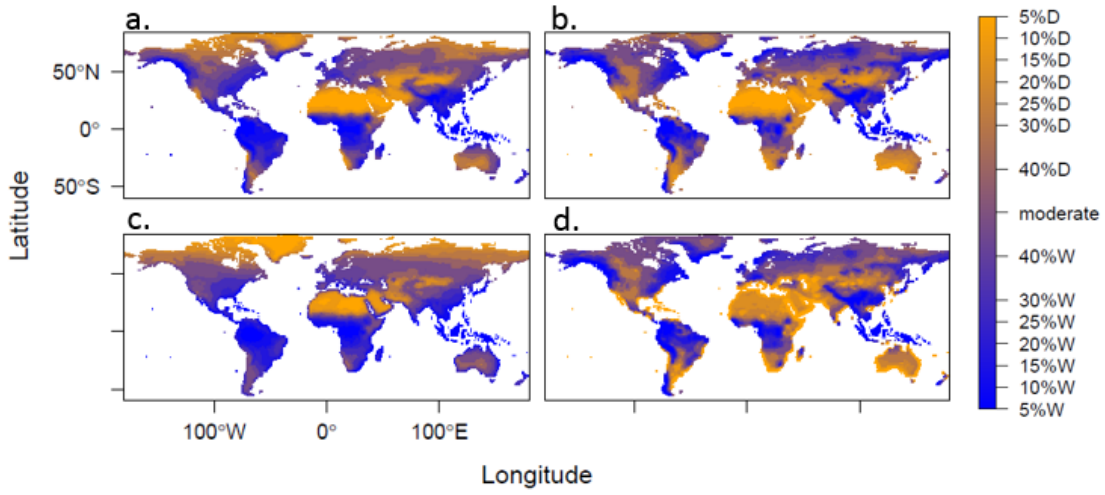

Figure 3.5 Wet and dry quantile plots base on the historic (1860-2005) average, where 5%W is the 5% wettest quantile, and 5% dry is the 5% driest quantiles for a) precipitation, b) runoff, c) evapotranspiration and d) precipitation-evapotranspiration.

The predicted slope is largest for the historically wettest quantiles, and incrementally decreases for the driest quantiles (Figure 3.6f, hereafter called the 'averaged model slope') for P-ET. We also see that the most negative slope (the largest decrease) is found in the driest regions globally (Figure 3.6f). We find that there are patterns WWDD at all quantiles (Figure 3.6f) where the most extreme wet (dry) areas have the most positive (negative) average global slopes.

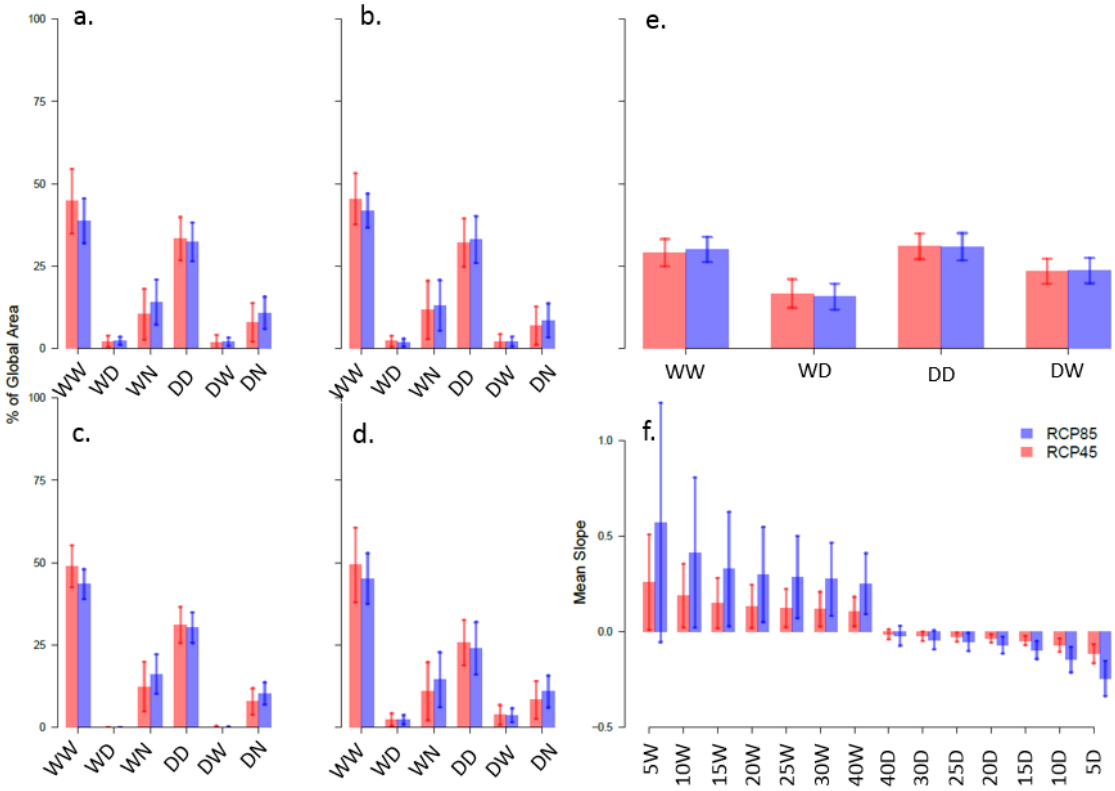

Figure 3.6 WWDD testing using the departure analysis (a) precipitation, b) runoff, c) evapotranspiration and d) precipitation-evapotranspiration) categorized by wet with wet departure (WW), wet with dry departure (WD), wet with no departure (WN), dry with dry departure (DD), dry with wet departure (DW) and dry with no departure (DN). Slope prediction analysis is completed for e) precipitation-evapotranspiration calculated on the historical 25% wettest and driest quantiles f) and mean slope of precipitation-evapotranspiration calculated on the suite of quantiles.

In testing the continuum WWDD pattern, we found that the magnitude of the spatially averaged slope was approximately linearly related to the quantile of P – ET over which we spatially averaged (Figure 3.6 f). All wet and dry quantiles showed similar patterns, with a slight decreasing trend in support for WWDD as quantiles increased.

3.4.3 Uncertainty Analysis

Most individual (54/58) projections (29 models under two forcing scenarios) exhibit WWDD trends as determined by the slope analysis, although there are a large range of magnitudes and distributions (Figure 3.7). Some models have much higher rates of P-ET, which may heavily weight the mean of model predictions. In particular, CCSM4,

CESM1-BGC, CESMI-CAM5, IPSL-CM5A-LR, IPSL-CM5A-MR, NorESM1-M and NORESM-MA exhibit a mean slope that is nearly double the mean slope of the remaining models (Figure 3.7). Some (5/58) individual models diverge from the expected WWDD pattern, with slopes for RCP4.5 and RCP8.5 predictions that have a different sign (ACCESS1-3, BNU-ESM, IPSL-CM5B-LR (for RCP4.5) (Figure 3.7)). For all models, the wet quantiles have a larger mean slope magnitude than the dry quantiles. For all quantiles in all models, the RCP8.5 slope magnitude is larger than the RCP4.5 magnitude, except for MRI-CGCM3. Of relevance to the inter-model analysis, the spatial distribution of the historic quantiles vary greatly between models, for (Supplement B.4) for both the historical 25% quantiles and the linear trend for both RCP4.5 and RCP8.5 (Figure 3.7).

All models under both RCP scenarios have a negative slope except for four (Figure 3.7b); specifically CSIRO-Mk3 (RCP4.5 and RCP8.5), BNU-ESM RCP4.5 and ACCESS1-3 RCP8.5. ACCESS1-3 and BNU-ESM were already identified as unusual with respect to the opposite sign of the slopes for RCP4.5 and RCP8.5 scenarios, and CSIRO-Mk-6-0 clearly does not follow the WWDD pattern in the wet quantiles (Figure 3.7 b). The standard error on the slope of quantile change is greater for RCP8.5 in 28/29 models, as well as being the more negative value in 25/29 models (Figures 3.7b). Overall, we find that most models (54/58) do exhibit the WWDD pattern for RCP4.5 and RCP8.5, indicating that the WWDD pattern is consistently present in global terrestrial CMIP5 simulations, although there are key differences between the models with respect to the magnitudes of slopes.

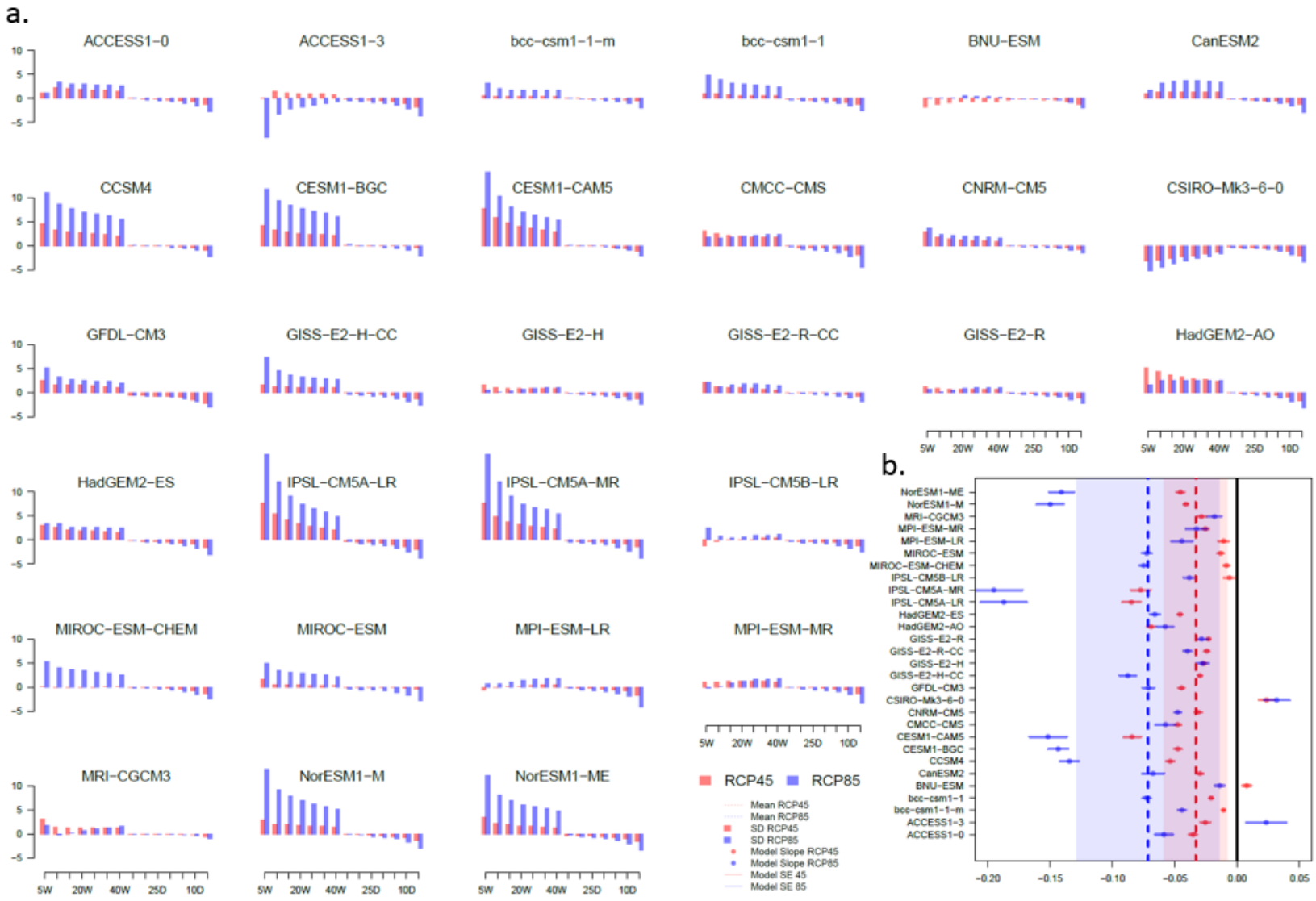

Figure 3.7 a) Trends in P-ET for 29 models shown with mean slope (predicted rate of change) of areas within the historic quantiles for RCP4.5 and RCP8.5 (2006-2100). b) Meta-analysis of the predicted slopes (of trends in 3.7 a) for RCP4.5 and RCP8.5 by model.

3.5 Discussion and Conclusion

Our analysis of CMIP5 model output for the terrestrial hydrological cycle provides a characterization of future hydrological budgets. We built upon existing research that examined these trends at the global scale which focused on the multi-model mean (Mora et al. 2014, Greve and Seneviratne 2015). Our analysis provided an expanded analysis of hydrological projections, focusing on inter-model variability and placing future projections in the context of historical variability using the concept of climate departure. We found that the departure analysis was a simple way of quantifying the predicted change for hydrological variables as well as a method that could be simply applied to test the WWDD hypothesis. Our results found stronger support across models (54/58 models support WWDD) for WWDD than previous results that used model means based solely on statistical significance.

We also found that there was not globally uniform agreement of departure among models, as shown in (Mora et al. 2013) using their controversial alternative definition of departure. In fact inter-model variability (in terms of both spatial pattern and absolute magnitude of change) was a primary characteristic of our results, indicating that the multi-model mean is not representative of individual projections. Fundamentally, this suggests that we collectively lack fundamental understanding of how the terrestrial water cycle may change in the future.

In terms of WWDD, we used an expanded departure framework to demonstrate stronger support for WWDD than did previous analyses. We believe the conclusions were different from previous studies that did not fund support for WWDD (Greve and Seneviratne 2015) for two primary reasons: one is that we utilized a *within-model* statistic (% of area that confirms/denies WWDD) that is independent of the spatial location of wet and dry regions and the absolute magnitude of change when comparing across models. Secondly, we analyzed 'significance' in the context of historical variability, as opposed to statistical p-values. Finally, by using a continuum of wet/dry definitions we were able to find support for across a continuum of quantiles which provides an extended WWDD framework where the spatially averaged slope was approximately linearly related to the

quantile over which we spatially averaged. We believe this provides additional support for the WWDD pattern.

Overall, our analysis suggests that there are fundamental structural uncertainties in our climate models that represent regional hydrological budgets into the future. Models appear highly variable in terms of the location and magnitude of change. However, we gleaned general patterns find that the WWDD is generally consistent across models, despite very little agreement as to where WWDD occurs. We thus suggest that inter-model comparison of future projections continue to be a central focus of hydrological research.

There are three limitations to this analysis. The first is the duration of the historical time scales. Longer durations (currently 1860-2005) would potentially increase the magnitude of the historical climate oscillations and make future projections more sensitive to departure. Following Mora et al. (2013) and Greve and Seneviratne (2015) we opted to use the core models to be consistent with the literature and we used the most models possible. Another limitation is the possibility that all models are not independent. Many models may share some underlying code and therefore not represent the same quantity of information as two independently developed models. While we do not infer statistical significance and therefore do not assume statistical independence, we do treat each model equally in calculating proportional model agreement and other results. Lastly, for this study we looked at annual trends, which may not tell a complete picture of hydrological climate change. Further work is recommended to examine seasonal and monthly trends to determine if climate departure and WWDD exist at a finer temporal scale.

Developing a clear physical picture of hydrological change into the future is fundamental for understanding local priorities and developing effective policy solutions. Encouragingly, inter-model comparison of Earth System models has already been cited as a central focus in hydrology and elsewhere, and a sixth phase of the Coupled Model Intercomparison Project (CMIP6) is already planned (Meehl et al. 2014). These models will be further gauged for their consistency in simulating regional hydrological budgets in an ongoing effort to understand and improve our quantitative understanding of the impacts of climate change.

CHAPTER 4 CONCLUSION

In this thesis, I examined and quantified two aspects of the global-scale hydrological budget. In Chapter 2, I focused on an empirical analysis of ET to better understand and quantify the drivers of ET and how these relationships vary with respect to LC types. This analysis advanced our understanding of global ET dynamics by synthesizing and modelling a new ET database of previously published observations. By explicitly accounting for LC type in the statistical models, the fits were better able to account for global ET variability and revealed significant global variation in its primary drivers as a function of LC type. In particular, we found that the effect of temperature, precipitation, and shortwave radiation were the most important set of predictors across all land types and that the effect of temperature and precipitation depended significantly on LC type, with precipitation having the strongest effect in barren lands and temperature having the strongest effect in lakes and inundated areas. These results will help us further constrain a highly uncertain global flux and better understand the consequences of LC change on the hydrological cycle which is occurring throughout the world.

In Chapter 3, I focused on future projections and analyzed computer model simulations of the future hydrological budget using output from an ensemble of global-scale earth models (i.e. CMIP5). Here I specifically structured the analysis of CMIP5 data to focus on future hydrological projections in the context of historical variability using the climate departure analysis first presented by Mora et al. (2013). The primary results here were strong regional variability in hydrological departure; in particular, a dichotomous departure response for wet vs. dry areas of the land surface. I found that wet areas of the world are predicted to depart their historical climate regime by getting wetter 21 times more often than getting drier, and that dry climates are predicted to depart their historical regime by getting drier 18 times more often than by getting wetter (for P-ET under RCP4.5). This result is in contrast to other analyses of Earth System models that looked at absolute trends in hydrological variables and found weaker support for the wet-get-wetter, dry-get-drier pattern (WWDD) than those found here. This comparison highlighted the importance for understanding natural climate variability in estimating hydrologically significant change over time. We further showed that the WWDD pattern exists over a continuum of wet/dry definitions for the land surface. This added further

robustness to the patterns previously seen in analyses of climate models and thus strengthens our confidence of this trend into the future, due to the robustness, and support of multiple models. However, a strong conclusion from the analysis was that CMIP5 models exhibit inconsistent spatial locations of wet and dry areas and large variations in the absolute magnitude of predicted change. Only when a location- and magnitude-independent statistic was applied did the WWDD pattern appear more consistently.

In terms of future work, Chapter 2 highlighted a general need for greater global coverage of empirical evapotranspiration observations. Specifically we found that the Arctic, Africa and central Asia are underrepresented in the ET observational literature. Chapter 2 also highlighted the importance of variations in ET by LC, and future work should further investigate and resolve patterns of ET by LC in observations and models so to better understand the hydrological consequences of LC change. Chapter 3 motivates significant further work into analyzing and reconciling inter-model variability in hydrological predictions. We recommend that future studies using CMIP5 and the future CMIP6 database diagnose global patterns of change by examining inter-model contrasts, as opposed to the multi-model mean, because fundamental model-model disagreement exists and must be reconciled before developing a consistent picture of future hydrological change.

In conclusion, the balance of the hydrological budget plays a fundamental role in governing planetary surface energy budgets, structuring terrestrial ecosystems, and ultimately determining the prosperity and sustainability of human society. The research in this thesis has provided an empirical and model-based analysis of regional variability in hydrological budgets at the global-scale. In doing so, this research aids in understanding the balance of regional hydrological budgets, the drivers of these fluxes, and how they may change into the future. As climate continues to evolve over the 21st century, changes to the hydrological cycle are expected to predict strong, yet highly uncertain, regional variability that will impact local communities and economies in diverse ways. This thesis expands our understanding of these changes and helps us place future change in the context of recent natural variability.

BIBLIOGRAPHY

Ajtay, G. L., P. Ketner, and P. Duvigneaud. 1979. Terrestrial Primary Production and Phytomass. Pages 129–181 *in* B. Bolin, E. . Degens, S. Kempe, and P. Ketner, editors. The Global Carbon Cycle. Wiley, New york.

Alkama, R., L. Marchand, A. Ribes, and B. Decharme. 2013. Detection of global runoff changes: results from observations and CMIP5 experiments. Hydrol. Earth Syst. Sci. 17:2967–2979.

Allan, R. P., B. J. Soden, V. O. John, W. Ingram, and P. Good. 2010. Current changes in tropical precipitation. Environ. Res. Letters 5:025205.

Arnell, N. W. 2004. Climate change and global water resources: SRES emissions and socio-economic scenarios. Global Environmental Change 14:31–52.

Arora, V. K. 2001. Streamflow simulations for continental-scale river basins in a global atmospheric general circulation model. Advances in Water Resources 24:775–791.

Baumgartner, A., E. Reichel, and R. Lee. 1975. World water balance : Mean annual global, continental and maritime precipitation, evaporation and run-off. Elsevier Scientific Publishing Co, Amsterdam.

Berner, E. K. 1987. The Global Water Cycle: Geochemistry and Environment. Prentice-Hall, Englewood Cliffs, New Jersey.

Boé, J., and L. Terray. 2008. Uncertainties in summer evapotranspiration changes over Europe and implications for regional climate change. Geophysical Research Letters 35:L05702.

Boisier, J. P., N. de Noblet-Ducoudré, and P. Ciais. 2014. Historical land-use induced evapotranspiration changes estimated from present-day observations and reconstructed land-cover maps. Hydrol. Earth Syst. Sci. Discuss. 11:2045–2089.

Bonan, G. B. 2010. Ecological Climatology: Concepts and Applications, 2nd Edition. Geographical Research.

Brutsaert, W. 2008. Hydrology: An Introduction. 3rd ed. Hydrology: An Introduction.

Caldwell, M. M., J. F. Bornman, C. L. Ballaré, S. D. Flint, and G. Kulandaivelu. 2007. Terrestrial ecosystems, increased solar ultraviolet radiation, and interactions with other climate change factors. Photochemical & photobiological sciences : Official journal of the European Photochemistry Association and the European Society for Photobiology 6:252–266.

Čermák, J., and A. Prax. 2009. Transpiration and soil water supply in floodplain forests. Ekológia (Bratislava) 28:248–254.

Chapin, F. S., P. A. Matson, and H. A. Mooney. 2002. Principles of Terrestrial Ecosystem Ecology. Springer.

Chou, C., J. C. H. Chiang, C.-W. Lan, C.-H. Chung, Y.-C. Liao, and C.-J. Lee. 2013. Increase in the range between wet and dry season precipitation. Nature Geoscience 6:263–267.

Chou, C., J. D. Neelin, C. A. Chen, and J. Y. Tu. 2009. Evaluating the "rich-get-richer" mechanism in tropical precipitation change under global warming. Journal of Climate 22:1982–2005.

Creed, I. F., A. T. Spargo, J. A. Jones, J. M. Buttle, M. B. Adams, F. D. Beall, E. Booth, J. Campbell, D. Clow, K. Elder, M. B. Green, N. B. Grimm, C. Miniat, P. Ramlal, A. Saha, S. Sebestyen, D. Spittlehouse, S. Sterling, M. W. Williams, R. Winkler, and H. Yao. 2014. Changing forest water yields in response to climate warming: Results from long-term experimental watershed sites across North America. Global change biology 20:3191–3208.

Dirmeyer, P. A., G. Fang, Z. Wang, P. Yadav, and A. D. Milton. 2014. Climate change and sectors of the surface water cycle in CMIP5 projections. Hydrology and Earth System Sciences Discussions 11:8537–8569.

Douville, H., A. Ribes, B. Decharme, R. Alkama, and J. Sheffield. 2013. Anthropogenic influence on multidecadal changes in reconstructed global evapotranspiration. Nature Climate Change 3:59–63.

Efron, B., and Rj. J. Tibshirani. 1994. An introduction to the bootstrap. CRC Press.

Elsner, M. M., L. Cuo, N. Voisin, J. S. Deems, A. F. Hamlet, J. a. Vano, K. E. B. Mickelson, S. Y. Lee, and D. P. Lettenmaier. 2010. Implications of 21st century climate change for the hydrology of Washington State. Climatic Change 102:225–260.

Erb, K.-H., V. Gaube, F. Krausmann, C. Plutzar, A. Bondeau, and H. Haberl. 2007. A comprehensive global 5 min resolution land-use data set for the year 2000 consistent with national census data. Journal of Land Use Science 2:191–224.

Gerten, D. 2013. A vital link: water and vegetation in the Anthropocene. Hydrol. Earth Syst. Sci. 17:3841–3852.

Greve, P., B. Orlowsky, B. Mueller, J. Sheffield, M. Reichstein, and S. I. Seneviratne. 2014. Global assessment of trends in wetting and drying over land. Nature Geoscience 7:716–721.

Greve, P., and S. I. Seneviratne. 2015. Assessment of future changes in water availability and aridity. Geophysical Research Letters 42.

Haddeland, I., D. B. Clark, W. Franssen, F. Ludwig, F. Voß, N. W. Arnell, N. Bertrand, M. Best, S. Folwell, D. Gerten, S. Gomes, S. N. Gosling, S. Hagemann, N. Hanasaki, R. Harding, J. Heinke, P. Kabat, S. Koirala, T. Oki, J. Polcher, T. Stacke, P. Viterbo, G. P. Weedon, and P. Yeh. 2011. Multimodel Estimate of the Global Terrestrial Water Balance: Setup and First Results. Journal of Hydrometeorology 12:869–884.

Hastie, T., R. Tibshirani, and J. Friedman. 2001. The Elements of Statistical Learning. Springer New York USA.

Hawkins, E., B. Anderson, N. Diffenbaugh, I. Mahlstein, R. Betts, G. Hegerl, M. Joshi, R. Knutti, D. McNeall, S. Solomon, R. Sutton, J. Syktus, and G. Vecchi. 2014. Uncertainties in the timing of unprecedented climates. Nature 511:E3–E5.

Held, I. M., and B. J. Soden. 2006. Robust responses of the hydrological cycle to global warming. Journal of Climate 19:5686–5699.

IPCC. 2013. Climate Change 2013: The Physical Science Basis. Contribution of Working Group I to the Fifth Assessment Report of the Intergovernmental Panel on Climate Change. (T. F. Stocker, D. Qin, G.-K. Plattner, M. Tignor, S. K. Allen, J. Boschung, A. Nauels, Y. Xia, V. Bex, and P. M. Midgley, Eds.) Cambridge University Press. Cambridge, United Kingdom and New York, NY, USA.

Jasechko, S., Z. D. Sharp, J. J. Gibson, S. J. Birks, Y. Yi, and P. J. Fawcett. 2013. Terrestrial water fluxes dominated by transpiration. Nature 496:347–50.

Jung, M., M. Reichstein, P. Ciais, S. I. Seneviratne, J. Sheffield, M. L. Goulden, G. Bonan, A. Cescatti, J. Chen, R. de Jeu, A. J. Dolman, W. Eugster, D. Gerten, D. Gianelle, N. Gobron, J. Heinke, J. Kimball, B. E. Law, L. Montagnani, Q. Mu, B. Mueller, K. Oleson, D. Papale, A. D. Richardson, O. Roupsard, S. Running, E. Tomelleri, N. Viovy, U. Weber, C. Williams, E. Wood, S. Zaehle, and K. Zhang. 2010. Recent decline in the global land evapotranspiration trend due to limited moisture supply. Nature 467:951–954.

Kadane, J. B., and N. A. Lazar. 2004. Methods and Criteria for Model Selection. Journal of the American Statistical Association 99:279–290.

Kimball, B. a., and S. B. Idso. 1983. Increasing atmospheric CO2: effects on crop yield, water use and climate. Agricultural Water Management 7:55–72.

Kröger, M. 2012. Global tree plantation expansion: a review. Netherlands.

Lambert, F. H., and M. J. Webb. 2008. Dependency of global mean precipitation on surface temperature. Geophysical Research Letters 35:1–5.

Lieth, H. 1972. Modelling the primary productivity of the world. Nature and Resources.

Lieth, H. 1975. Primary Production of the Major Vegetation Units of the World. Pages 203–215 Primary Productivity of the Biosphere.

Liu, C., and R. P. Allan. 2013. Observed and simulated precipitation responses in wet and dry regions 1850–2100. Environmental Research Letters 8:034002.

Lu, J., and M. Cai. 2009. Seasonality of polar surface warming amplification in climate simulations. Geophysical Research Letters 36:1–6.

McCabe, M. F., E. F. Wood, R. Wójcik, M. Pan, J. Sheffield, H. Gao, and H. Su. 2008. Hydrological consistency using multi-sensor remote sensing data for water and energy cycle studies. Remote Sensing of Environment 112:430–444.

Meehl, G. A., R. Moss, K. E. Taylor, V. Eyring, R. J. Stouffer, S. Bony, and B. Stevens. 2014. Climate Model Intercomparisons: Preparing for the Next Phase. Eos, Transactions American Geophysical Union 95:77–78.

Miralles, D. G., J. H. Gash, T. R. H. Holmes, R. A. M. de Jeu, and A. J. Dolman. 2010. Global canopy interception from satellite observations. Journal of Geophysical Research 115:D16122.

Monteith, J. L. 1965. Evaporation and environment. Pages 205–234 Symposia of the Society for Experimental Biology. University Press.

Mora, C., A. G. Frazier, R. J. Longman, R. S. Dacks, M. M. Walton, E. J. Tong, J. J. Sanchez, L. R. Kaiser, Y. O. Stender, J. M. Anderson, C. M. Ambrosino, I. Fernandez-Silva, L. M. Giuseffi, and T. W. Giambelluca. 2013. The projected timing of climate departure from recent variability. Nature 502:183–187.

Mora, C., A. G. Frazier, R. J. Longman, R. S. Dacks, M. M. Walton, E. J. Tong, J. J. Sanchez, L. R. Kaiser, Y. O. Stender, J. M. Anderson, C. M. Ambrosino, I. Fernandez-Silva, L. M. Giuseffi, and T. W. Giambelluca. 2014. Mora et al. reply. Nature 511:E5–E6.

Mu, Q., M. Zhao, and S. W. Running. 2011. Improvements to a MODIS global terrestrial evapotranspiration algorithm. Remote Sensing of Environment 115:1781–1800.

Mueller, B., M. Hirschi, C. Jimenez, P. Ciais, P. A. Dirmeyer, A. J. Dolman, J. B. Fisher, M. Jung, F. Ludwig, F. Maignan, D. Miralles, M. F. McCabe, M. Reichstein, J. Sheffield, K. C. Wang, E. F. Wood, Y. Zhang, and S. I. Seneviratne. 2013. Benchmark products for land evapotranspiration: LandFlux-EVAL multi-dataset synthesis. Hydrol. Earth Syst. Sci. Discuss. 10:769–805.

Mueller, B., S. I. Seneviratne, C. Jimenez, T. Corti, M. Hirschi, G. Balsamo, P. Ciais, P. Dirmeyer, J. B. Fisher, Z. Guo, M. Jung, F. Maignan, M. F. McCabe, R. Reichle, M. Reichstein, M. Rodell, J. Sheffield, A. J. Teuling, K. Wang, E. F. Wood, and Y. Zhang. 2011. Evaluation of global observations-based evapotranspiration datasets and IPCC AR4 simulations. Geophysical Research Letters 38:L06402.

Ngo-Duc, T., J. Polcher, and K. Laval. 2005. A 53-year forcing data set for land surface models. Journal of Geophysical Research: Atmospheres 110:D06116.

Oki, T. 1999. The global water cycle. Pages 10–27 *in* K. Browning and R. Gurney, editors. Global Energy and Water Cycles. Cambridge University Press.

Olson, J. S. 1975. Productivity of Forest Ecosystems. Pages 33–43 Productivity of World Ecosystems. National Academy of Sciences, Seattle.

Olson, J. S., J. A. Watts, and L. J. Allison. 1983. Carbon in live vegetation of major world ecosystems. ORNL.

Palmer, M. A., C. A. Reidy Liermann, C. Nilsson, M. Flörke, J. Alcamo, P. S. Lake, and N. Bond. 2008. Climate change and the world's river basins: Anticipating management options. Frontiers in Ecology and the Environment 6:81–89.

Piao, S., P. Friedlingstein, P. Ciais, N. de Noblet-Ducoudré, D. Labat, and S. Zaehle. 2007. Changes in climate and land use have a larger direct impact than rising CO2 on global river runoff trends. Proceedings of the National Academy of Sciences 104:15242–15247.

Pinheiro, J. C., and D. M. Bates. 2000. Mixed-Effects Models in S and S-PLUS. Springer, New York.

Ramankutty, N., and J. A. Foley. 1999. Estimating historical changes in global land cover: Croplands from 1700 to 1992. Global Biogeochemical Cycles 13:997–1027.

Rockström, J., L. Gordon, C. Folke, M. Falkenmark, and M. Engwall. 1999. Linkages among water vapor flows, food production, and terrestrial ecosystem services. Conservation Ecology 3:5.

Saugier, B., J. Roy, and H. A. Mooney. 2001. Estimations of global terrestrial productivity: Converging towards a single number? Pages 543–558 Terrestrial Global Productivity.

Seneviratne, S. I., T. Corti, E. L. Davin, M. Hirschi, E. B. Jaeger, I. Lehner, B. Orlowsky, and A. J. Teuling. 2010. Investigating soil moisture–climate interactions in a changing climate: A review. Earth-Science Reviews 99:125–161.

Seneviratne, S. I., D. Lüthi, M. Litschi, and C. Schär. 2006. Land-atmosphere coupling and climate change in Europe. Nature 443:205–9.

Shukla, J., and Y. Mintz. 1982. Influence of Land-Surface Evapotranspiration on the Earth's Climate. Science 215:1498–1501.

Sterling, S., and A. Ducharne. 2008. Comprehensive data set of global land cover change for land surface model applications. Global Biogeochemical Cycles 22:GB3017.

Sterling, S. M., A. Ducharne, and J. Polcher. 2013. The impact of global land-cover change on the terrestrial water cycle. Nature Climate Change 3:385–390.

Teuling, A. J., S. I. Seneviratne, R. Stockli, M. Reichstein, E. Moors, P. Ciais, S. Luyssaert, B. van den Hurk, C. Ammann, C. Bernhofer, E. Dellwik, D. Gianelle, B. Gielen, T. Grunwald, K. Klumpp, L. Montagnani, C. Moureaux, M. Sottocornola, and G. Wohlfahrt. 2010. Contrasting response of European forest and grassland energy exchange to heatwaves. Nature Geoscience 3:722–727.

United States Geological Survey. 1997. Earth Resources Observation and Science Center. http://eros.usgs.gov/elevation-products.

Vorosmarty, C. J., P. B. McIntyre, M. O. Gessner, D. Dudgeon, A. Prusevich, P. Green, S. Glidden, S. E. Bunn, C. A. Sullivan, C. R. Liermann, and P. M. Davies. 2010. Global threats to human water security and river biodiversity. Nature 467:555–561.

Wunsch, C. 1999. The interpretation of short climate records, with comments on the North Atlantic and Southern Oscillations. Bulletin of the American Meteorological Society 80:245–255.

Yin, Y., S. Wu, and E. Dai. 2010. Determining factors in potential evapotranspiration changes over China in the period 1971–2008. Chinese Science Bulletin 55:3329–3337.

Zeng, Z., S. Piao, X. Lin, G. Yin, S. Peng, P. Ciais, and R. B. Myneni. 2012. Global evapotranspiration over the past three decades: estimation based on the water balance equation combined with empirical models. Environmental Research Letters 7:014026.

Zhang, X., F. W. Zwiers, G. C. Hegerl, F. H. Lambert, N. P. Gillett, S. Solomon, P. A. Stott, and T. Nozawa. 2007. Detection of human influence on twentieth-century precipitation trends. Nature 448:461–465.

APPENDIX A

A.1. GETA 2.0 Point Locations

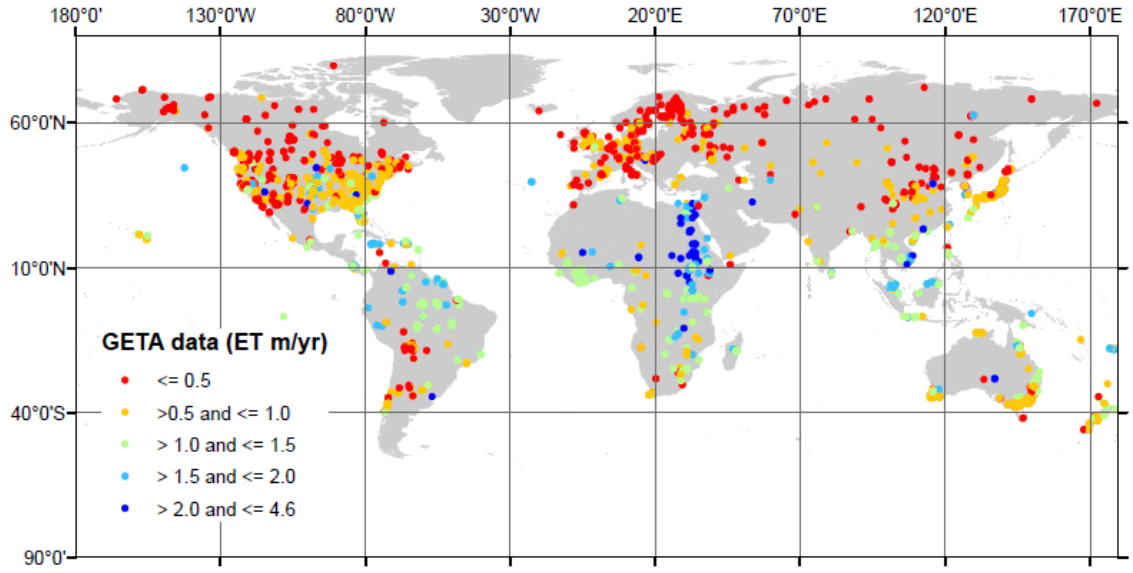

Figure A.1 Location of GETA 2.0 points, classified by rates of ET (m/yr).

A.2. Precipitation bounds on ET

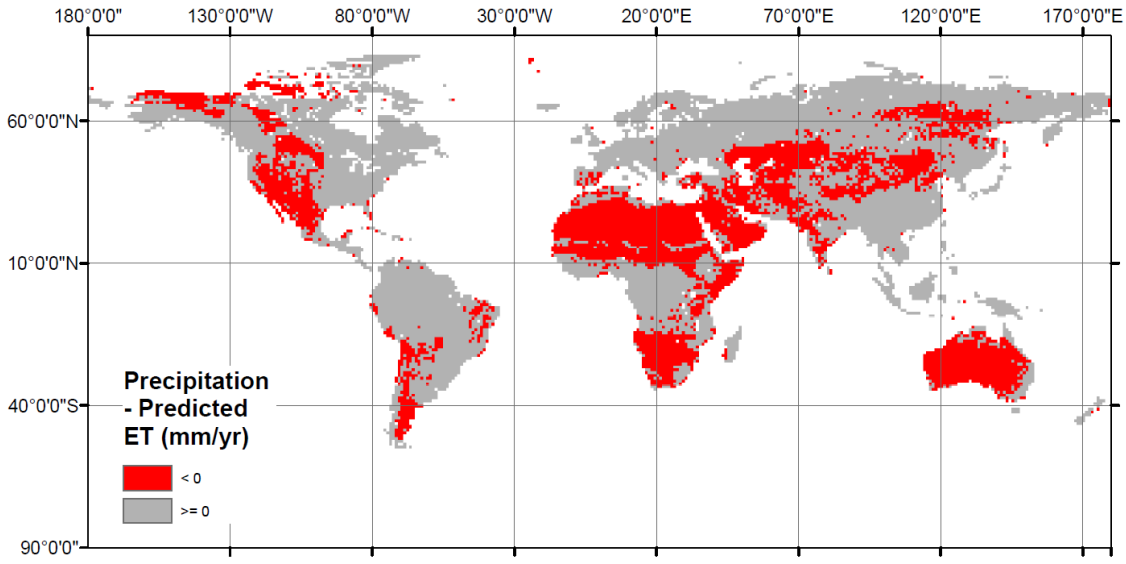

Figure A.2 Areas where predicted rates of ET (ET_LMM) are greater than averaged precipitation (53-yr annual forcing dataset).

A.3. Spatial Prediction Uncertainties by Independent Predictor Variables

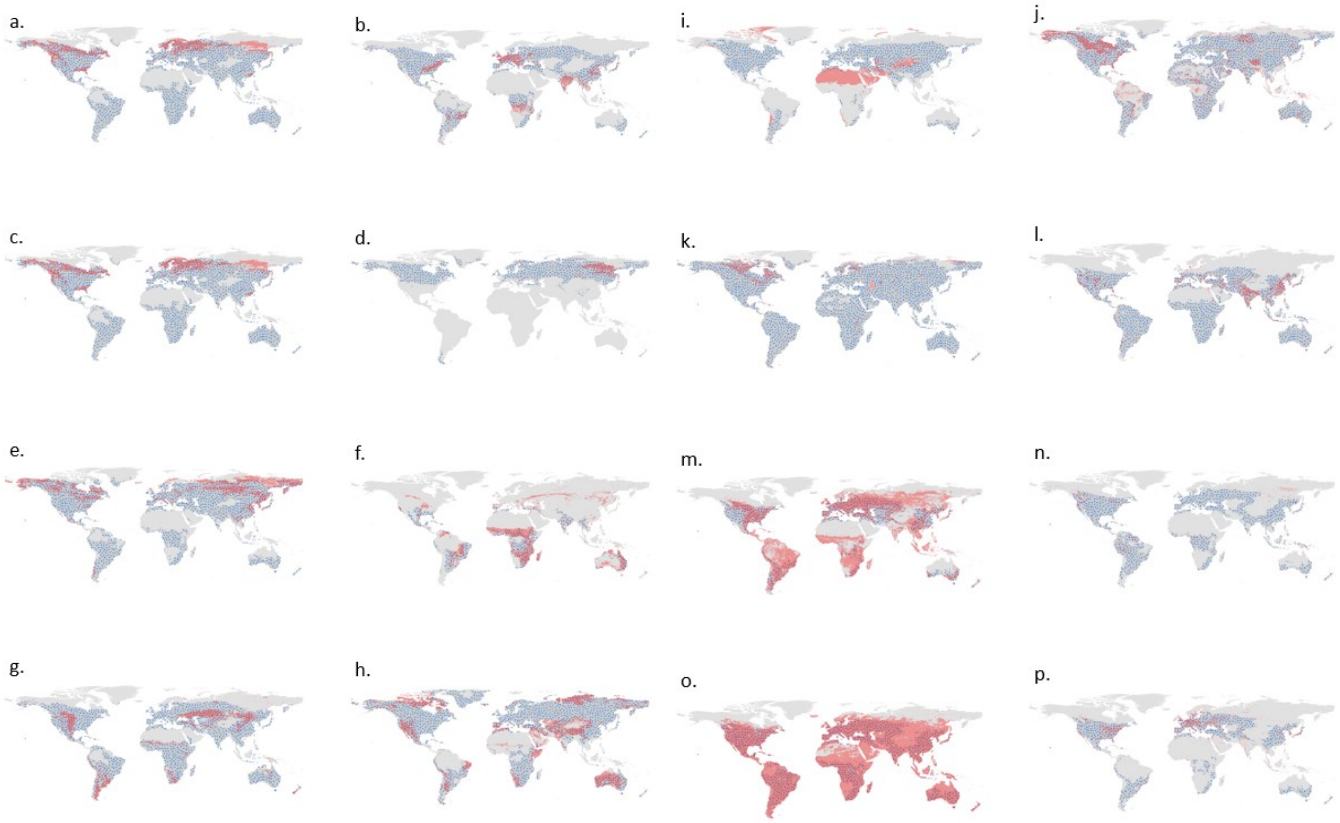

Figure A.3 Range of LC's (red) and intersection of independent predictors (blue dots) where there is coverage of all three (temperature, precipitation, short wave radiation). a. ENF, b. DBF, c. ENF, d. DNF, e. MXF, f. SAV, g. GRS, h. SHR, i. BAR, j. WTL, k. LAK, l. CRI, m. CRN, n. TPL, o. GRZ, p. HMO.

APPENDIX B

B.1. CMIP5 Models Used in Departure and WWDD Analysis

Table B.1 Models used in analysis for precipitation (Precip), Runoff (Runoff), Evapotranspiration (ET), and Precipitation-ET (P-ET).

Center	Country	Model	Precip	Runoff	ET	P-ET
Commonwealth Scientific and Industrial Research Organisation	Australia	ACCESS1-0	X	X	X	X
		ACCESS1-3	X	X	X	X
Beijing Climate Center, China Meteorological Administration	China	bcc-csm1-1-m	X	X	X	X
		bcc-csm1-1	X	X	X	X
College of Global Change and Earth System Science, Beijing Normal University	China	BNU-ESM	X	X	X	X
Canadian Centre for Climate Modelling and Analysis	Canada	CanESM2	X	X	X	X
National Center for Atmospheric Research	United States	CCSM4	X	X	X	X
National Science Foundation	United States	CESM1-BGC	X	X	X	X
		CESM1-CAM5	X	X	X	X
Centro Euro-Mediterraneo per I Cambiamenti Climatici	Italy	CMCC-CM	X		X	X
		CMCC-CMS			X	
Centre National de Recherches Meteorologiques / Centre Europeen de Recherche et Formation Avancees en Calcul Scientifique	France	CNRM-CM5	X	X	X	X
Commonwealth Scientific and Industrial Research Organization with Queensland Climate Change Centre of Excellence	Australia	CSIRO-Mk3-6-0	X	X	X	X
EC-Earth Consortium	Europe	EC-EARTH		X	X	
First Institute of Oceanography	China	FIO-ESM	X			
NOAA Geophysical Fluid Dynamics Laboratory	United States	GFDL-CM3	X	X	X	X
NASA Goddard Institute for Space Studies	United States	GISS-E2-H-CC	X	X	X	X
		GISS-E2-H	X	X	X	X
		GISS-E2-R-CC	X	X	X	X
		GISS-E2-R	X	X	X	X
National Institute of Meterological Research/Korea Meterological Administration	Korea	HadGEM2-AO	X	X	X	X
Met Office Hadley Centre	UK	HadGEM2-ES	X		X	X
Institute for Numerical Mathematics	Russia	inmcm4	X	X		
Institut Pierre-Simon Laplace	France	IPSL-CM5A-LR	X	X	X	X
		IPSL-CM5A-MR	X	X	X	X
		IPSL-CM5B-LR	X	X	X	X
Japan Agency for Marine-Earth Science and Technology, Atmosphere and Ocean Research Institute (The University of Tokyo), and National Institute for Environmental Studies	Japan	MIROC-ESM-CHEM	X	X	X	X
		MIROC-ESM	X	X	X	X
Atmosphere and Ocean Research Institute (The University of Tokyo), National Institute for Environmental Studies, and Japan Agency for Marine-Earth Science and Technology	Japan	MIROC5	X	X		
Max Planck Institute for Meteorology	Germany	MPI-ESM-LR	X	X	X	X
		MPI-ESM-MR	X	X	X	X
Meteorological Research Institute	Japan	MRI-CGCM3	X	X	X	X
Norwegian Climate Centre	Norway	NorESM1-M	X	X	X	X
		NorESM1-ME	X	X	X	X
Total			32	30	31	29

B.2. Departure at 50% model agreements

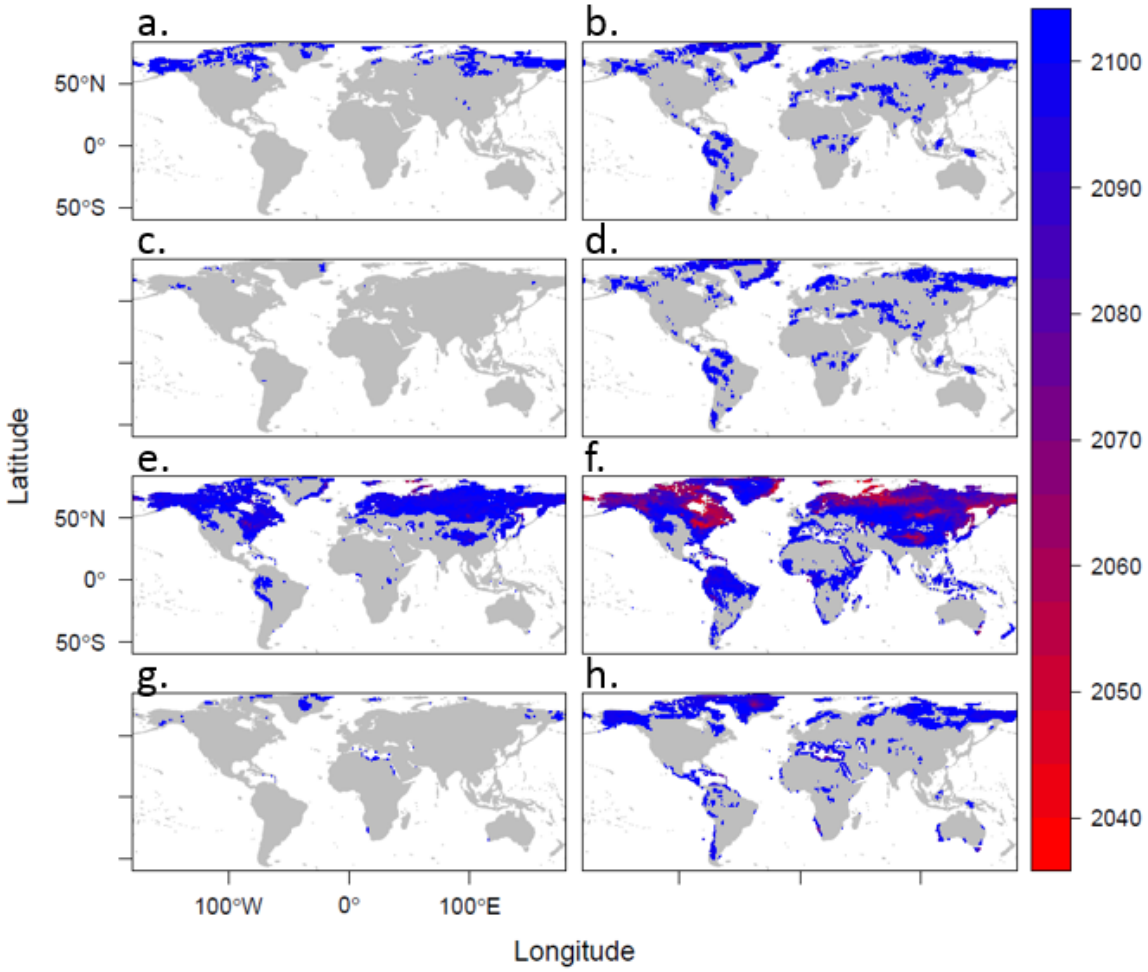

Figure B.1 Date of historic departure when 50% of models agree for a) precipitation RCP4.5, b) precipitation RCP8.5, c) runoff RCP4.5, d) runoff RCP8.5, e) evapotranspiration RCP4.5, f) evapotranspiration RCP8.5, g) precipitation-evapotranspiration RCP4.5, and precipitation-evapotranspiration RCP8.5.

B.3. WWDD Slope Analysis across continuum of slopes

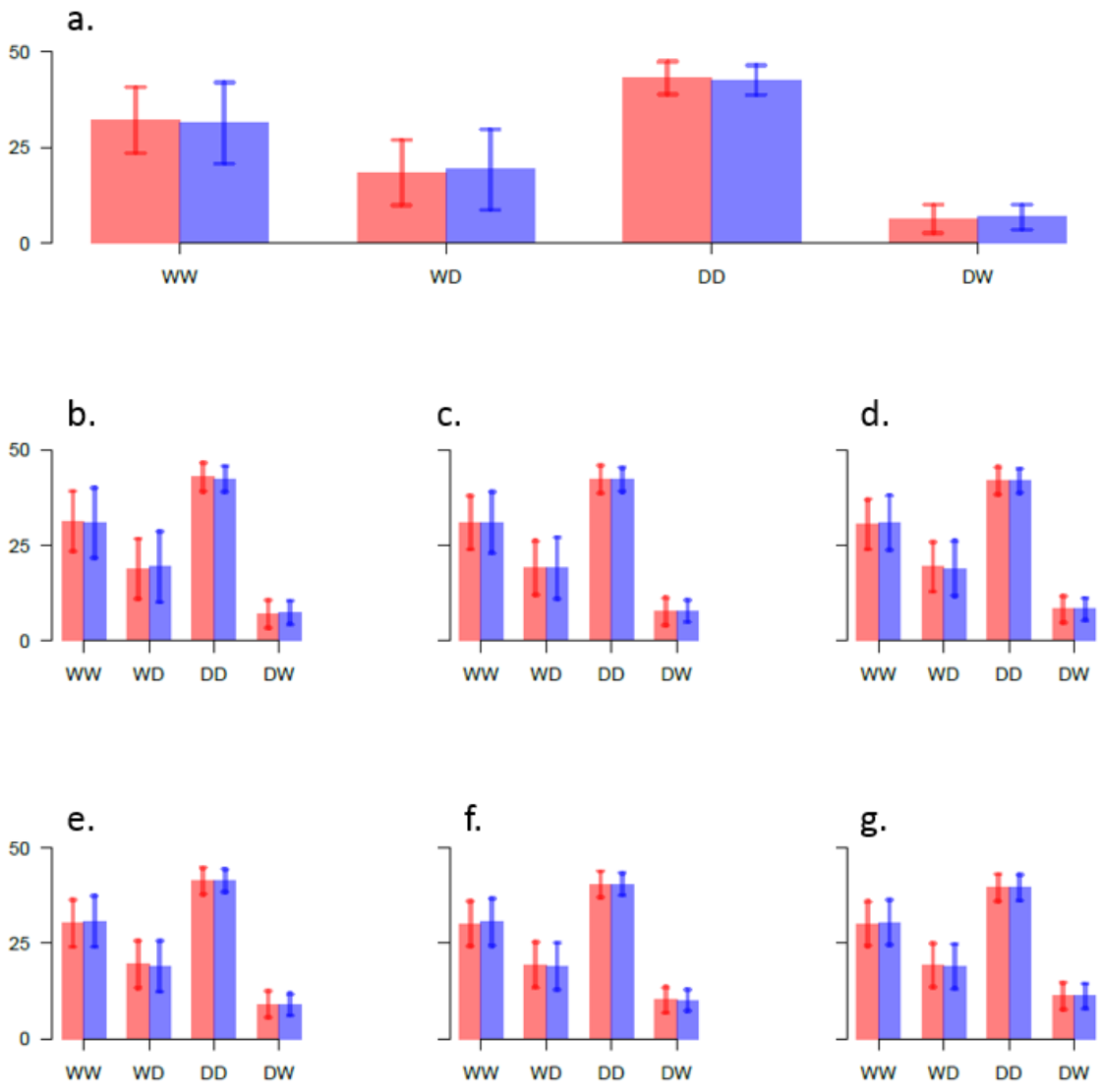

Figure B.2 Direction of change for the historically wettest and driest quantiles (a. 5%, b. 10%, c. 15%, d. 20%, e. 25%, f. 30%, g. 40%) completed using a slope analysis for P-ET for RCP4.5 (red) and RCP8.5 (blue).

B.4. WWDD Slope Analysis

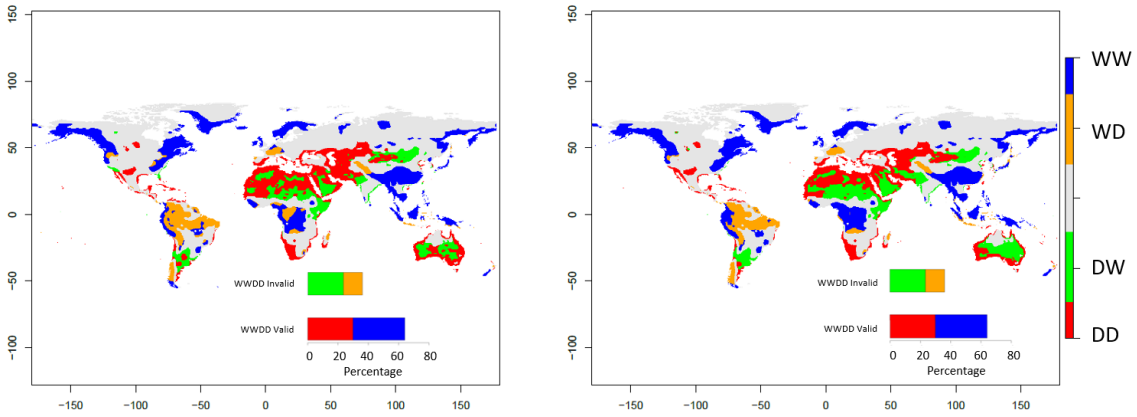

Figure B.3 Direction of change for the historically 25% wettest and driest quantiles determined by P-ET. Completed using slope analysis for P-ET for RCP4.5 (left) and RCP8.5 (right).

B.5. Historic Quantiles by Model

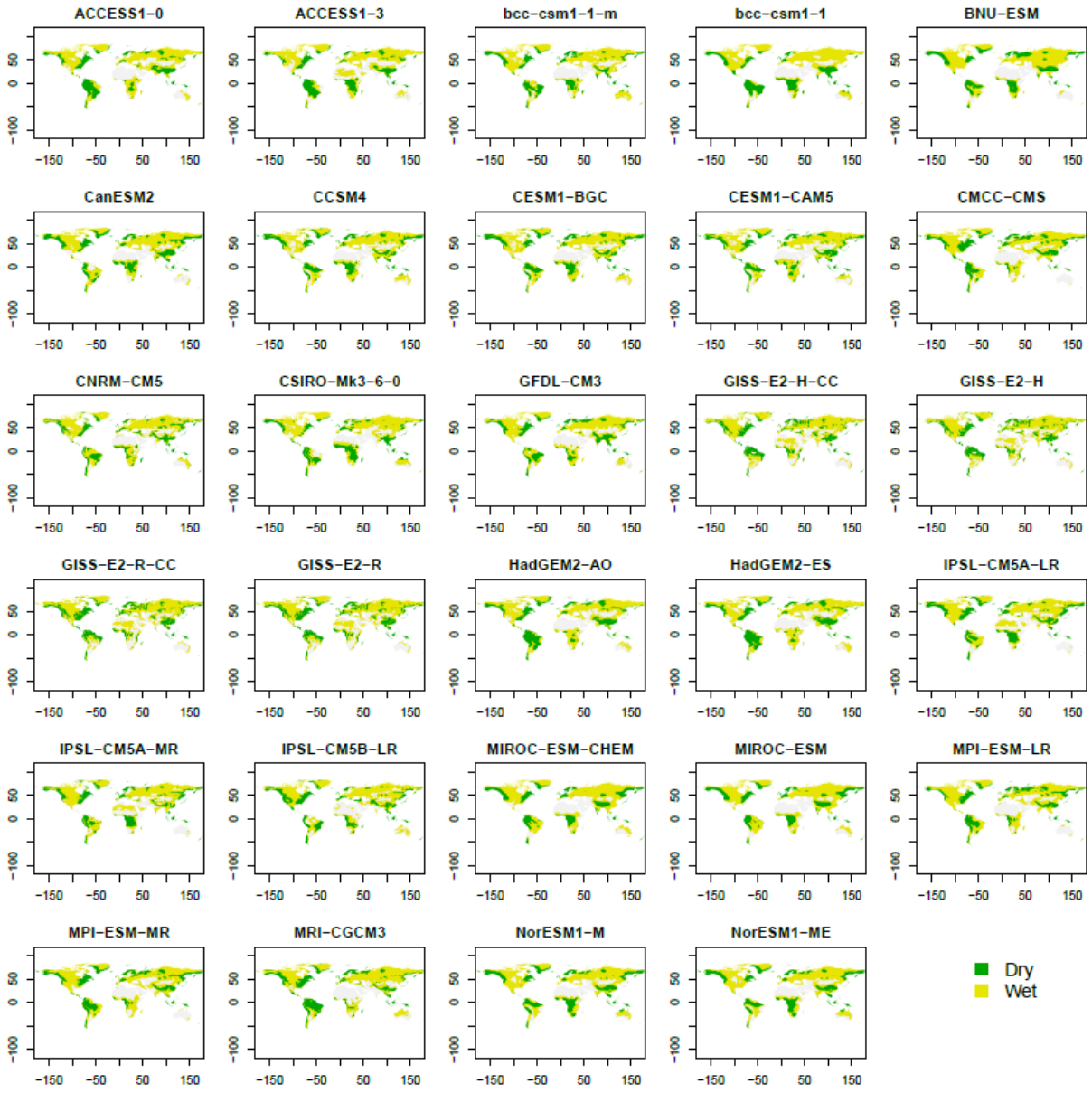

Figure B.4 Historical quantiles of wet (green) and dry (yellow), defined as P-ET, regions determined by the 25% top wettest and driest quantiles between 1860 and 2005.